

Present-day scaling relations of submm galaxies: origin of spheroidal sytems

T. Takagi^{1,2,3,4*}, H. Hanami⁵ and N. Arimoto^{6,7}

¹ Centre for Astrophysics and Planetary Science, University of Kent, Canterbury, Kent, CT2 7NR, UK

² Blackett Laboratory, Imperial College, Prince Consort Road, London, SW7 2BZ, UK

³ The Institute of Space and Astronautical Science, 3-1-1 Yoshinodai, Sagamihara, Kanagawa 229-8510, Japan

⁴ Department of Physics, Rikkyo University, 3-34-1 Nishi-Ikebukuro, Toshima-ku, Tokyo 171-8501, Japan

⁵ Physics Section, Faculty of Humanities and Social Sciences, Iwate University, Morioka, 020-8550, Japan

⁶ Institute of Astronomy, School of Science, University of Tokyo, 2-21-1 Osawa, Mitaka, Tokyo 181-0015, Japan

⁷ National Astronomical Observatory, 2-21-1 Osawa, Mitaka, Tokyo 181-8588, Japan

ABSTRACT

We analyse the spectral energy distributions (SEDs) of 23 submm galaxies and 3 *ISO*-detected EROs, all of which have the spectroscopic redshifts, by using an evolutionary SED model of starbursts. This SED model allows us to investigate intrinsic properties of starbursts, such as the starburst age and the mean stellar metallicity, as it takes into account the chemical evolution. Also, the intrinsic size of the starburst region is estimated from observed SEDs. Using this SED model, we predict colour, magnitude, and size of present-day descendants of submm galaxies, and derive scaling relations, such as the present-day colour-magnitude and size-magnitude relations. We argue that submm galaxies are the progenitors of present-day elliptical galaxies, provided that the initial mass function (IMF) of submm galaxies is slightly flatter than the Salpeter IMF. In this case, we find that 1) the mean present-day magnitude of submm galaxies is similar to that of L^* elliptical galaxies, 2) the present-day colour-magnitude relation is consistent with that of elliptical galaxies, 3) the present-day size-magnitude relation of elliptical galaxies can be reproduced if massive submm galaxies consist of multiple starburst regions. We estimate the effect of feedback in submm galaxies as a function of starburst age. It is found that starburst regions in submm galaxies are likely to be self-regulated; i.e. the effect of feedback is nearly balanced with the self-gravity of starburst regions.

Key words: galaxies: starburst – dust, extinction – infrared: galaxies – ultraviolet: galaxies – submillimetre.

1 INTRODUCTION

Submillimetre (submm) galaxies are the key to understand the process of galaxy formation (e.g. Smail, Ivison & Blain 1997; Hughes et al. 1998; Eales et al. 1999; Scott et al. 2002). It has been found that submm galaxies are massive starburst galaxies at high redshifts; i.e. gas mass is estimated to be as large as $\sim 10^{11} M_\odot$ from the CO line emission (Frayer et al. 1998, 1999; Ivison et al. 2001; Genzel et al. 2003; Neri et al. 2003), and the median redshift of $z = 2.4$ is recently found spectroscopically (Chapman et al. 2003a). If observed submm fluxes originate mainly from star formation, the star formation rates (SFRs) of bright submm galaxies are estimated to be over $10^3 M_\odot \text{ yr}^{-1}$ (e.g. Smail et al. 2002; Chapman et al. 2003a), large enough to produce a massive

elliptical galaxy ($L > 3 L^*$) within ~ 1 Gyr (comparable to the Hubble time at $z = 2.5$). This estimate seems to be confirmed with the follow-up observations at X-ray, which suggest the negligible contribution of the AGN to submm fluxes (Alexander et al. 2003). These observations indicate that submm galaxies are the most plausible candidates of the progenitors of present-day elliptical galaxies.

The evolutionary link between submm galaxies and elliptical galaxies is also suggested by the statistical properties of submm galaxies. The comoving number density of submm galaxies with the $850 \mu\text{m}$ flux of $> 8 \text{ mJy}$ is comparable to that of present-day ellipticals with $L \sim 3 - 4 L^*$ (Chapman et al. 2003a). Another clue to the evolutionary link could be given by the clustering properties of submm galaxies, which should be strong if they are the progenitors of massive elliptical galaxies. This would be tested by large submm surveys in near future.

* E-mail: t.takagi@kent.ac.uk

Theoretically, the semi-analytic methods (SAMs) are extensively applied to explain the statistical properties of elliptical galaxies (e.g. Baugh et al. 1996; Kauffmann et al. 1996; Cole et al. 2000; Benson et al. 2001; Diaferio et al. 2001; Springel et al. 2001). The SAMs show that most of massive galaxies are formed at $z \lesssim 1$ as a result of successive merging of smaller objects. Therefore, it is difficult to explain the statistical properties of submm galaxies with the standard SAMs. This problem comes from the uncertainty in the relation between the dynamical evolution of the dark matter and the star formation processes in the early stage of galaxy formation (e.g. Binney 2004). In order to avoid this uncertainty, we may need an alternative method to investigate the evolutionary link between submm galaxies and elliptical galaxies.

Elliptical galaxies are known as a fairly homogeneous family; e.g. they exhibit very small scatter in the colour-magnitude relation (e.g. Bower et al. 1992) and the relation between the Mg_2 index and the velocity dispersion σ (Dressler et al. 1987), i.e., their properties are well characterized as a sequence of mass. It is also remarkable that they occupy a two-dimensional sheet (fundamental plane) in the three dimensional space defined by the velocity dispersion σ , the effective radius r_e , and the mean surface brightness within r_e (Dressler et al. 1987; Djorgovski & Davis 1987). If submm galaxies evolve into elliptical galaxies, their present-day properties must be consistent with these scaling relations. This kind of test can provide the other piece of evidence for the evolutionary link between submm galaxies and elliptical galaxies.

In this paper, we analyse submm galaxies with an evolutionary model of spectral energy distribution (SED) for starburst galaxies, which is presented by Takagi, Arimoto & Hanami (2003a; hereafter TAH03). In this model, the chemical evolution of starburst region is considered; i.e. if we specify the evolutionary phase of submm galaxies as starbursts, gas mass and stellar mass of submm galaxies can be estimated, together with their chemical abundances. Also, the intrinsic size of starburst region can be estimated from the observed SEDs, since the geometry of starburst region determines its optical depth for a given dust mass. By using this model, we predict the present-day colour, magnitude and size of submm galaxies from observed SEDs, and produce the present-day scaling relations for submm galaxies, i.e. the colour-magnitude relation and the size-magnitude relation. Then, these scaling relations are compared with those of elliptical galaxies, in order to prove the evolutionary link between submm galaxies and elliptical galaxies. This approach is new and complementary to the previous studies.

The structure of this paper is as follows. We describe practical methods of SED diagnostics of submm galaxies in Section 2. We summarise the results of SED fitting in Section 3. We confront the predicted present-day characteristics of submm galaxies with those of present-day elliptical galaxies in Section 4. Then, we discuss a possible evolutionary scenario of submm galaxies in Section 5. Our conclusions are given in Section 6. Throughout this paper, we adopt the cosmology of $\Omega_m = 0.3$, $\Omega_\Lambda = 0.7$ and $H_0 = 75 \text{ km sec}^{-1} \text{ Mpc}^{-1}$.

2 PRESCRIPTION OF SED DIAGNOSTICS FOR SUBMM GALAXIES

2.1 Evolutionary SED model of submm galaxies

We consider the evolution of starburst regions in submm galaxies. Each starburst region is assumed to be a dynamically isolated system in which the chemical enrichment proceeds with effective mixing of gas by supernova feedback. The SED of such starburst region is determined by the starburst age for a given star formation history and the spatial distribution of stars and dust, i.e. geometry. The adopted SED model is the same as the model applied to nearby starbursts in TAH03, except for the initial metallicity and the initial mass function (IMF). Here we briefly describe this SED model.

2.1.1 Evolutionary model of starburst regions

We approximate the star formation history in a starburst region with an infall model of Arimoto, Yoshii & Takahara (1992). In this model, the overall star formation history is described with two time-scales, i.e. the gas infall time-scale t_i and the star formation time-scale t_* . We adopt the simplest case, in which a starburst is characterized by only one evolutionary time-scale t_0 , i.e., we assume $t_i = t_* \equiv t_0$. Thus, we specify the star formation history with t_0 , which is important only for the absolute time-scale of starburst events. Note that the chemical evolution as a function of t/t_0 is almost independent of the practical choice of t_0 (TAH03). Since this is also true for the properties of the SED, specifically when $t_0 \gtrsim 50 \text{ Myr}$, we can derive the chemical properties of starbursts from the observed SED, irrespective of the adopted value of t_0 (i.e. the star formation history). Practically, all models are calculated with $t_0 = 100 \text{ Myr}$. Once the starburst age (t/t_0) is specified with the total mass of initial gas M_T , we can derive the gas mass M_g and stellar mass M_* in the starburst region, together with the metallicities of gas and stars.

We assume that the metallicity of pre-galactic gas clouds Z_i is negligibly small (i.e. $Z_i=0$). It is possible that pre-galactic gas clouds are chemically enriched with the former star formation activity. However, our conclusions are independent of practical choice of Z_i when $Z_i \lesssim 0.1 Z_\odot$.

A simple model of dust evolution is adopted; i.e. we assume that the dust-to-metal ratio δ_0 is constant. The value of δ_0 depends on the dust model. We adopt three dust models, i.e. the model for dust in the Milky Way (MW), LMC and SMC. For the MW, LMC and SMC, the values of δ_0 derived from the extinction curve and the spectra of cirrus emission are 0.40, 0.55, and 0.75, respectively. See TAH03 and Takagi, Vansevičius, & Arimoto (2003b) in detail.

2.1.2 Geometry of starburst regions

We assume that stars in submm galaxies are centrally concentrated as those in elliptical galaxies. The stellar density distribution is given by the King profile with $\log(R_t/R_c) = 2.2$ where R_t and R_c are the cut-off and core radius, respectively, and the adopted value is typical for elliptical galaxies (Combes et al. 1995). As in TAH03, dust is assumed to distribute homogeneously within R_t .

Note that TAH03 show that the effective radii of ultraluminous infrared galaxies (ULIRGs) derived from SEDs are consistent with the observed ones at J , H , and K -band. In this geometry, the longer the observed wavelength, the smaller the observed effective radius, so far as the observed flux is dominated by stellar emissions. This is because stars in the central region contribute to the observed flux more and more with decreasing the optical depth. TAH03 also show that this trend is consistent with the observations of ULIRGs. Therefore, the adopted geometry is found to be suitable for nearby ULIRGs.

Since the amount of dust is given by the chemical evolution, the geometry of starburst region determines the optical depth by dust. Therefore, one of the important parameters of this SED model is a compactness factor Θ of starburst regions, defined by

$$\frac{R_t}{1\text{kpc}} = \Theta \left(\frac{M_*}{10^9 M_\odot} \right)^\gamma, \quad (1)$$

where $\gamma = 1/2$ is adopted, resulting in the constant surface brightness for constant Θ . Note that the SED feature is preserved for different values of M_* when $\gamma = 1/2$, since the source function within the starburst is conserved.

The optical depth of starburst regions, here defined with the column density of dust measured from the centre to outer edge, is a function of starburst age and Θ . By using M_* and Θ derived from the SED fitting, we calculate the intrinsic effective radius R_e (i.e. effective radius with no dust)¹, which is given by $10.75 \times R_c$ in the adopted geometry.

In Section 4.2, we point out that massive submm galaxies may consist of multiple starburst regions. So far, photometric data are available only for a whole galaxy especially at longer wavelengths. Therefore, it is difficult to analyse the SED of each starburst region. If the SED of starburst regions in submm galaxies is similar to each other, the derived starburst age and Θ for a whole galaxy can be interpreted as those of each starburst region. This condition is such that each starburst is triggered almost simultaneously and the intrinsic bolometric surface brightness of each starburst region is similar to each other, like nearby self-regulated starbursts (TAH03).

2.1.3 Evolution of stellar populations

A population synthesis code developed by Kodama & Arimoto (1997) is used to calculate the spectral evolution of stellar populations. In this model, the effects of stellar metallicity are explicitly taken into account in spectra. This is important to consistently calculate spectra of passively evolving galaxies, which mainly depend on the metallicity and the age of stellar population (Worthey 1994).

We adopt the two IMFs, i.e. the Salpeter IMF with the power law index of $x = 1.35$ (IMF_{1.35}), and a top-heavy IMF with the flatter slope $x = 1.10$ (IMF_{1.10}). Such a flat IMF has been suggested by Kodama & Arimoto (1997) for elliptical galaxies, and found for the OB associations in the Milky Way (Massey et al. 1995). For both the IMFs, we

adopt the lower and upper mass limit of $0.1 M_\odot$ and $60 M_\odot$, respectively.

The choice of IMF is important for the present-day magnitudes of submm galaxies, since the mass-to-light ratio is smaller for the flatter IMF. Also, the present-day colours of submm galaxies depend on the IMF, since the yield of chemical enrichment is higher for the flatter IMF.

2.1.4 Radiative transfer with dust

The SED from UV to submm of starburst regions is calculated for each starburst age, Θ and the extinction curve (MW, LMC and SMC), by using the code for the radiative transfer used by TAH03. In this code, isotropic multiple scattering is assumed and the self-absorption of re-emitted energy from dust is fully taken into account. The temperature of dust grains is calculated for each dust size and constituent at each radial grid. For very small grains, the temperature fluctuation is calculated consistently with the radiative transfer. See Takagi et al. (2003b) in detail.

2.2 Sample galaxies

The sample includes extremely red objects (EROs) detected at the MIR–submm wavelengths, submm galaxies found with SCUBA blank field surveys, submm galaxies amplified by the gravitational lens, submm galaxies in the proto-cluster region, and host galaxies of gamma-ray bursts (GRBs) detected at the submm wavelengths. Although 3 of *ISO*-detected EROs do not have observed flux at submm wavelengths, we call the sample galaxies as submm galaxies for simplicity.

We consider submm galaxies which have spectroscopic redshifts only. Therefore, the secure optical identification is inevitable. The spectroscopic redshift is necessary to significantly reduce the uncertainty of the SED fitting.

Also, the sample galaxies need to have extensive photometric data enough to perform the SED fitting. We consider galaxies which have more than 3 photometric data in the optical-NIR bands². In total, we collect 23 galaxies detected at submm wavelengths and 3 *ISO*-detected EROs from the literature (including private communication). The observed properties of the sample galaxies are summarised in Table 1. In Appendix A, we summarise the observations of the sample galaxies. For SMMJ02399-0136, we perform the SED fitting with two possible optical counterparts L1 and L2 (Ivison et al. 1998).

2.3 SED-fitting method

The best-fitting SED model is searched by the χ^2 minimization technique from a prepared set of SED models. We calculate the SED models for 10 different starburst ages ($t/t_0 = 0.1 - 6.0$) and 16 different compactness factors

¹ Hereafter, we simply use the term ‘effective radius’ for this meaning in this paper.

² Although 2 GRB hosts have only 2 optical-NIR photometric data, we find that the constraint on the model parameters is acceptable. This is because the observed SEDs are rather peculiar, which is reproduced only with very young and optically thick SED models. Therefore, we include these galaxies in the sample.

($\Theta=0.3-3.0$) for each type of extinction curve; i.e. the best-fitting SED model is selected from a total of 480 SED models. This model set is made for both IMF_{1.35} and IMF_{1.10}. The upper limits of flux are taken into account in the fitting process, i.e. models exceeding the 3σ upper limits are simply rejected.

3 RESULTS OF SED FITTING

The fitting results with IMF_{1.35} and IMF_{1.10} are summarised in Table 2a and 2b, respectively. The results of SED fitting are shown in Figure 1 for IMF_{1.10} which is more suitable for submm galaxies than IMF_{1.35} (see section 4). Note that the fitting parameters are t/t_0 and Θ with the choice of the extinction curve. The normalization of the SED model is adjusted by M_T . The rest quantities are derived from the best-fitting SED model. In Appendix B, we show the contour maps of $\Delta\chi^2$ for the sample used in the main analysis given in Section 4 and 5. Also, the typical values of estimated errors are shown in Figure 2, 4, and 6.

Table 3 summarises the results of SED fitting, giving the number of galaxies for each bin of age and optical depth, and the resulting extinction curve. We find that 45 % of submm galaxies have $t/t_0 \leq 1$, in a marked contrast to nearby starbursts, showing only ~ 23 % have $t/t_0 \leq 1$. Thus, a significant fraction of submm galaxies are found to be young. The optical depth τ_V of submm galaxies has a peak at $10-20$, which is similar to that of nearby ULIRGs (cf. TAH03).

The large fraction of apparently young starbursts in submm galaxies may be caused by an extra AGN contribution to the rest-frame UV light. Since we have no further information on the presence of AGN for most of submm galaxies, we hereafter assume that they are intrinsically young. This assumption does not change our main conclusions which are derived from old ($t/t_0 \geq 2.0$) submm galaxies.

EROs detected in the MIR – submm wavelengths are found to be the oldest starburst galaxies ($t/t_0 \gtrsim 5$) in the sample. This means that colours of stellar populations should be intrinsically red, in order to reproduce extremely red colours. Note that the derived stellar masses for EROs are systematically higher than those of the other sample, due to higher mass-to-light ratio.

GRB host galaxies (2 out of 3) have unique SEDs characterized by young stellar populations ($t/t_0 < 1$) and large optical depth ($\tau_V \sim 60$). Although their optical depths are the largest among our sample, the optical/NIR SEDs are not very red. This is because only stars near the surface of the starburst region actually contribute to the observed UV-NIR SED in such a large τ_V .

Spectroscopic observations and X-ray detections suggest that 6 sample galaxies (EROJ164023, ISOJ1324-2016, PDFJ011423, CUDSS14.13, SMMJ02399-0136 and SMMJ02399-0134) harbour AGN. As a result of SED fitting, we find a clear MIR excess over the SED model for 4 sources (EROJ164023, PDFJ011423, CUDSS14.13, and SMMJ02399-0134) out of 6, which can be attributed to hot dust components around AGNs. On the other hand, the observed MIR fluxes of the other sample (HR10, CUDSS14F, and CUDSS14A) are reasonably explained solely by the starburst SED model. When the observed SEDs, except for the

MIR excess, are well explained by the SED model, we assume that AGN dominates only at MIR wavelengths, and therefore the derived parameters are still usable for the following analysis.

For 4 sample galaxies (EROJ164023, N2 850.1, SMMJ123629.13+621045.8, SMMJ131225.7+424350), we find no reasonable SED fit; i.e. SED models significantly under-estimate the fluxes at MIR and submm wavelengths even if they give good fit to the optical-NIR SEDs. The possible reasons are 1) the contamination from AGN (EROJ164023), 2) the uncertainty in the optical identification (N2 850.1), and 3) the low signal-to-noise ratio for faint objects (SMMJ131225.7+424350 with $S_{850\mu\text{m}} = 2.4 \pm 0.74$ mJy). For SMMJ123629.13+621045.8, it seems that none of these reasons is suitable. Note that SMMJ123629.13+621045.8 is one of the reddest object ($R-K=6.7$). We may need to extend the parameter range to fit such an extremely red SED. Accordingly, we exclude these 4 galaxies in the following analysis.

We present the fitting results of SMMJ02399-0136 for both L1 and L2. Since the relative contribution to MIR-submm flux from each component is uncertain due to the large beam size of telescopes, we assumed that the observed MIR-submm flux is dominated by either L1 or L2. If the observed dust emission is dominated by L2, the flux at rest-frame $2\mu\text{m}$ is significantly under-estimated, while the flux at rest-frame $4\mu\text{m}$ is properly reproduced. It is difficult to explain this discrepancy with the presence of hot dust component around the AGN. On the other hand, the SED of L1 component is reproduced well by the model. Therefore, we hereafter assume that observed dust emission originates mainly from the L1 component.

4 PRESENT-DAY SCALING RELATIONS OF SUBMM GALAXIES

4.1 Present-day color-magnitude relation of submm galaxies

The present-day colours and magnitudes are calculated under the assumption that effects of star-formation after the observed epoch are not significant for the resulting present-day colours and magnitudes. This assumption is safe specifically for starbursts in the later evolutionary phase; at $t/t_0 \sim 2$, about 60 % of mass in the gas reservoir is already transformed into stars.

In Figure 2, we compare the predicted present-day colours ($U-V$) and magnitudes of submm galaxies with the colour-magnitude (CM) relation of elliptical galaxies at $z=0$. In this figure, a solid curve with crosses indicates the present-day colour and magnitude of a starburst at $z=3$ with $M_T = 10^{12} M_\odot$, which corresponds to the formation of the brightest elliptical galaxy. If the predicted present-day magnitude is lower than that indicated by this line at a given $U-V$, present-day descendants of submm galaxies (or simply end-products) would be more massive than brightest elliptical galaxies.

In the case of IMF_{1.35}, more than half of old ($t/t_0 \geq 2$) submm galaxies are more massive than the brightest elliptical galaxies. Moreover, the resulting $U-V$ colours of all sample galaxies are bluer than the CM relation. In order to

reddden the end-products, a significant amount of metal rich stars or old stars (i.e. red stars) should be additionally supplied. Since the stellar mass is already comparable to that of the brightest elliptical galaxies, such scenarios to supply red stars are not plausible. Therefore, we suggest that IMF_{1.35} are not appropriate for submm galaxies.

On the other hand, in the case of IMF_{1.10}, the majority of old submm galaxies are less massive than the brightest elliptical galaxies. We derive the mean $V(B)$ -band magnitude of -22.03 (-20.97) mag for old submm galaxies. Thus, the typical luminosity of the end-products of these submm galaxies is similar to those of L^* elliptical galaxies which have $M_B^* = -20.75$ mag (Marinoni et al. 1999).

For IMF_{1.10}, not only the magnitudes, but also the present-day colours of old submm galaxies are consistent with those of elliptical galaxies; i.e. old submm galaxies seem to follow the CM relation. This suggests that these submm galaxies can be real progenitors of elliptical galaxies.

Note that young ($t/t_0 < 2$) submm galaxies are systematically bluer than old ($t/t_0 \geq 2$) ones. This is because we assume that the star formation ceases at the observed epoch, irrespective of derived starburst ages, and therefore the mean metallicity of stars in young submm galaxies is smaller than that of old ones.

The observations of passively evolving elliptical galaxies suggest that the origin of CM relation is the systematic difference in the mean metallicity of stars rather than that in the mean age of stars (Kodama & Arimoto 1997). Here we can check the origin of the CM relation independently of the previous studies. In Figure 3, we show the present-day age and the luminosity-weighted metallicity as a function of present-day V -band magnitude. The scatter of age is considerable at all magnitudes. Such a large dispersion in age has recently been confirmed by Yamada et al. (2004) among elliptical galaxies in low density environments with a detailed study of $H\gamma_\sigma$ absorption index (Vazdekis & Arimoto 1999). Therefore, three luminous submm galaxies ($M_V \leq -21.5$) with the age of < 8 Gyr and $z \leq 0.85$ could be real progenitors of young field ellipticals. In Table 4, we give the mean characteristics of old submm galaxies at $z = 0$ for each bright ($M_V < -22$) and faint sample ($M_V \geq -22$). Although faint sample of old submm galaxies appears to be young in the mean value, we find no difference in the mean age when we include young submm galaxies (open circles in Figure 3). Note that the present-day age depends mainly on the redshift, not on the starburst age, while the present-day magnitude depends on the starburst age. If the end-products of young submm galaxies remains to be faint ($M_V \geq -22$), there is no systematic difference in the present-day age between bright and faint sample. On the other hand, we find the systematic difference in the mean luminosity-weighted metallicity, $\Delta \log(Z_*/Z_\odot) = 0.19$. Thus, the CM relation of elliptical galaxies could be caused by the systematic difference in the metallicity. However, we need more faint sample of old submm galaxies to derive firm conclusions on this issue.

The analyses of the observed CM relation of elliptical galaxies suggest that the major star formation of elliptical galaxies occurred at $z > 2$ (e.g. Bower et al. 1992; Kodama et al. 1998; Stanford et al. 1998). This suggests that the progenitor of elliptical galaxies would be found mostly at $z \gtrsim 2$. On the other hand, the mean redshift of our sample is 1.6, while

recent spectroscopic observations of submm galaxies suggest the median redshift of $z \sim 2.4$ (Chapman et al. 2003a). Our sample is likely to be biased towards low redshifts, since they should be bright enough in the optical/NIR photometric bands to perform the spectroscopic observations and also the SED fitting. Therefore, our sample occupies a lower tail of the redshift distribution of submm galaxies. Nevertheless, the present-day colours and magnitudes of the sample are consistent with the observed CM relation. This suggests that the physical mechanisms to establish the CM relation are still effective even at $z \lesssim 2$.

4.2 Present-day size-magnitude relation of submm galaxies

We compare the present-day B -band magnitudes and effective radii of submm galaxies with the observed relation for elliptical galaxies, so-called the Kormendy relation. Since IMF_{1.10} is more suitable for submm galaxies as shown above, we mainly focus on this case. The effective radii of old submm galaxies range from ~ 300 pc to a few kpc. As shown in Figure 4a, the predicted effective radii of less massive galaxies with $M_B \sim -19$ mag are consistent with the observed ones, while those of massive galaxies are an order of magnitude smaller than the observed ones.

This discrepancy in R_e for massive galaxies can be explained if the starburst region in submm galaxies are a multiple system rather than a unit system; i.e. several starburst regions are distributed within the potential of a whole galaxy, and these starburst regions eventually merge to form a more diffuse stellar system. Note that the recent observations of submm galaxies with the Hubble Space Telescope (*HST*) actually show the multiple structures (Chapman et al. 2003b). As we note in Section 2.1.2, the interpretation of the SED fitting remains the same if each starburst region is triggered almost simultaneously, and the intrinsic bolometric surface brightness of each starburst region is similar to each other.

The other possibility which may account for this discrepancy is that the stellar system expands, owing to dynamical response to gas removal as a galactic wind. Following Yoshii & Arimoto (1987), we find that old submm galaxies could expand by no more than factor of ~ 3 , irrespective of the time-scale of gas removal. Moreover, this effect is expected to be more significant for less massive galaxies. However, the discrepancy of effective radius between submm galaxies and elliptical galaxies is larger for more massive submm galaxies. Therefore, it is difficult to explain the discrepancy of R_e only by the dynamical response of a stellar system to the gas removal.

The size-magnitude relation of submm galaxies seems to deviate from that of elliptical galaxies around $M_B \sim -19.5$ mag; i.e. the largest starburst regions in submm galaxies probably have the present-day magnitude of only $M_B \sim -19.5$ mag. The number of starburst regions can be estimated from the present-day magnitudes if submm galaxies with the present-day $M_B = -19.5$ mag are the largest starburst regions. Submm galaxies with the L^* present-day luminosity are likely to have at least ~ 3 starburst regions within the size of effective radius ~ 5 kpc. The clumpiness of submm galaxies may correlate with the mass of submm galaxies, since the discrepancy of the radius is larger for

more massive submm galaxies. It is important to confirm the existence of the maximum scale in starburst regions, in order to understand the star formation process at high redshifts. To do this, we need high resolution imaging, e.g. with the Atacama Large Millimeter Array (ALMA).

If submm galaxies consist of multiple starburst regions, we need to correct the derived R_e for the multiplicity and for the effect of merging of these starburst regions, in order to compare the derived R_e with the effective radius of elliptical galaxies. To estimate the correction factor for these effects, we simply assume that starburst regions in a submm galaxy have a similar mass and SED to each other. We call this assumption as the ‘equality’ condition of the starburst region. We hereafter denote the stellar mass and the effective radius of each starburst region as m_* and r_e , respectively. When a submm galaxy consists of N starburst regions, we can write $r_e \sim R_e/\sqrt{N}$, since $m_* = M_*/N$ and $R_e \propto (Nm_*)^{1/2}$. The gravitational energy per unit mass in a starburst region is $\frac{Gm_*}{r_e} \sim \frac{GM_*}{\sqrt{N}R_e}$. If the gravitational energy per unit mass does not change during the assembly process of multiple starburst regions, and the total stellar mass is conserved, massive submm galaxies would eventually evolve into elliptical galaxies with the effective radius of $\sim \sqrt{N}R_e$; i.e. we need the correction factor \sqrt{N} for effective radii in Figure 4a. In Figure 4b, we show the size-magnitude relation corrected for the multiplicity. Note that the corrected size-magnitude relation has the similar slope with the observed size-magnitude relation of elliptical galaxies. The zero point is marginally consistent with the observation within the uncertainty, although it is systematically lower by a factor of ~ 2 . The difference in the zero point might be explained by the expansion of stellar system, as a result of the gas removal from each starburst region at the end of its activity (e.g. Yoshii & Arimoto 1987).

5 EVOLUTION OF SUBMM GALAXIES

The starburst activity can be characterized by the relative strength of self-gravity to feedback (TAH03). In massive and compact starbursts like nearby ULIRGs, the self-gravity of starburst region becomes strong enough to suppress the feedback effect. This is because the supernova rate depends mainly on the total baryonic mass of starburst regions, while the self-gravity increases with decreasing the size of starburst region for a given mass. First, we investigate the relative strength of self-gravity to feedback in submm galaxies, which can provide an insight into the evolution of submm galaxies.

5.1 Feedback versus self-gravity in submm galaxies

TAH03 estimate the strength of feedback from the kinetic energy of gas per unit mass. We follow the same prescription as that in TAH03. The total kinetic energy of gas due to feedback with the typical velocity V_g can be written as $\frac{1}{2}M_g V_g^2 \simeq L_{\text{kin}} t_{\text{dyn}}$, where L_{kin} is the kinetic luminosity due to feedback, and t_{dyn} is the dynamical time-scale of the system. Assuming that $L_{\text{kin}} = f_{\text{kin}} L_{\text{bol}}$ and $t_{\text{dyn}} = t_0$, the kinetic energy per a unit mass can be written as

$$\frac{1}{2}V_g^2 \simeq \frac{L_{\text{kin}} t_{\text{dyn}}}{M_g} = f_{\text{kin}} \frac{L_{\text{bol}}}{\psi}, \quad (2)$$

where $\psi (= M_g/t_0)$ is the SFR. We use the relation

$$\frac{L_{\text{bol}}}{\varepsilon L_\odot} = \frac{\psi}{1M_\odot \text{yr}^{-1}} \left(\frac{t}{t_0} \right)^\alpha \quad (3)$$

where we find $\varepsilon = (1.7 \times 10^9, 7.0 \times 10^9)$ and $\alpha = (1.0, 0.42)$ for $\text{IMF}_{1.35}$ and $\text{IMF}_{1.10}$. Then, we derive the escape velocity, $V_{\text{esc}}^2 \simeq 2GM(< R_e)/R_e$, where $M(< R_e)$ is the total mass within R_e . Here, we simply assume $f_{\text{kin}} = 0.01$ and $M(< R_e) = 2M_*(< R_e)$ as in TAH03. The limiting effect of feedback against self-gravity can be estimated by the comparison of V_g with V_{esc} . These velocities should be corrected when submm galaxies consist of N starburst regions. For the equality condition of starbursts, we find the escape velocity of each starburst region $v_{\text{esc}}^2 \simeq V_{\text{esc}}^2/\sqrt{N}$, since $m_* = M_*/N$ and $r_e \simeq R_e/\sqrt{N}$. On the other hand, we expect the velocity of gas due to feedback in each starburst $v_g \simeq V_g$, since the strength of feedback mainly depend on the efficiency of star formation, not on the mass scale. Therefore, we find $v_g^2/v_{\text{esc}}^2 \simeq \sqrt{N}V_g^2/V_{\text{esc}}^2$. If starbursts are self-regulated, we expect $v_g^2/v_{\text{esc}}^2 \gtrsim 1$.

In Figure 5, we show v_g^2/v_{esc}^2 corrected for the multiplicity, and find that most of old submm galaxies have $v_g^2/v_{\text{esc}}^2 \gtrsim 1$. This suggests that feedback is effective, and therefore the star formation in old submm galaxies is likely to be self-regulated.

In the local universe, TAH03 suggest that UV-selected starburst galaxies (UVSBGs) are self-regulated, while ULIRGs are dynamically unstable. The difference between UVSBGs and ULIRGs can be seen as a systematic difference in the intrinsic bolometric surface brightness. In Figure 6, we show the bolometric luminosity L_{bol} and the effective radius R_e of submm galaxies, along with those of nearby starburst galaxies. An arrow in Figure 6 indicates the correction due to the multiplicity, assuming the equality condition of starbursts and $N = 3$. The intrinsic bolometric surface brightness of old submm galaxies are systematically lower than those of nearby ULIRGs which have $> 10^{13} L_\odot \text{kpc}^{-2}$; instead, it seems to follow the relation of UVSBGs. Again, this may indicate that old submm galaxies are self-regulated starbursts. Thus, the effect of feedback could be very important for the evolution of submm galaxies.

5.2 Role of feedback and origin of the CM relation

The evolutionary trend of the feedback effect in submm galaxies can be seen in Figure 7, which shows v_g^2/v_{esc}^2 of submm galaxies (corrected for the multiplicity) as a function of starburst age t/t_0 . For old submm galaxies, v_g^2/v_{esc}^2 is found to be almost constant (~ 1). Thus, feedback in submm galaxies is nearly balanced with the self-gravity for $t/t_0 \gtrsim 1$. This means that the starburst activity in submm galaxies could easily cease at any starburst age.

Even so, the star formation activity would not completely cease when starburst regions reside in a large scale gravitational potential well, probably due to dark matter, since the gas can fall back again to starburst regions. Note that such dark matter haloes are necessary to explain the surface brightness profile at X-ray from nearby elliptical

galaxies (e.g. Trinchieri, Fabbiano & Canizares 1986; Matsushita et al. 1998). This also means that the mixing of gas could occur in the scale of dark matter halo; i.e. the chemical evolution in multiple starburst regions may be related to each other.

We suggest that massive submm galaxies consist of multiple self-regulated starbursts in the dark matter halo. In such systems, how the starburst activity ceases is determined not by the properties of the starburst itself, but by the gravitational potential of the dark matter halo. This means that both the resulting stellar mass and the stellar metallicity are controlled by the gravitational potential of the dark matter halo. This may be important to explain the tightness of the CM relation of elliptical galaxies.

6 CONCLUSIONS

We analyse submm galaxies, including EROs and host galaxies of GRBs, by using the evolutionary SED model of starburst galaxies. This model allows us to investigate the intrinsic properties of submm galaxies as starbursts, since the chemical evolution is consistently taken into account. We determine the evolutionary phase of submm galaxies, and derive the stellar mass and the metallicity of stars. Then, we predict the colour, magnitude and size of present-day descendants of submm galaxies, based on the results of the SED fitting. This prediction is more reliable for old submm galaxies ($t/t_0 \gtrsim 2$), since the large fraction of gas would have been already used to form stars, and therefore the effect of star formation after the observed epoch is not significant.

We derive the present-day scaling relations of submm galaxies; i.e. the colour-magnitude and the size-magnitude relations at $z = 0$. These scaling relations can provide new clues on the evolutionary link between submm galaxies and elliptical galaxies. By comparing them with the observed scaling relations of elliptical galaxies, we have reached the following conclusions:

- The predicted present-day colours and magnitudes of submm galaxies suggest that the IMF of submm galaxies is flatter than $\text{IMF}_{1.35}$; otherwise the present-day magnitude of submm galaxies become brighter than the brightest elliptical galaxies.
- With $\text{IMF}_{1.10}$, the predicted colours and magnitudes of old submm galaxies are consistent with the observed CM relation of elliptical galaxies. The mean present-day magnitude of submm galaxies is similar to that of L^* elliptical galaxies. This implies that these submm galaxies are quite likely to evolve into present-day elliptical galaxies after the starburst event.
- The derived effective radii of less massive submm galaxies ($M_B \sim -19$ mag at $z = 0$) are consistent with the observed size-magnitude relation of elliptical galaxies. The small size of massive submm galaxies, compared with the size of ellipticals with similar mass, suggests that they consist of multiple starburst regions. When the multiplicity of starburst regions is taken into account, the resulting effective radii become consistent with the observation within the uncertainty.

Furthermore, we find that starbursts in submm galaxies are self-regulated; i.e. feedback is nearly balanced with the

self-gravity. This mechanism may be important to explain the tightness of the colour-magnitude relation of elliptical galaxies.

ACKNOWLEDGEMENTS

TT would like to thank to N. Shibazaki, V. Vansevicius, T. Matsumoto, M. Rowan-Robinson and G. White for their encouraging supports. We are grateful to the referee S. Chapman for providing valuable data which significantly improve the quality of the paper. This work was financially supported in part by a Grant-in-Aid for the Scientific Research (No.11640230, 13011201, 13640230 & 14540220) by the Japanese Ministry of Education, Culture, Sports and Science. This research has been supported in part by a Grant-in-Aid for the Center-of-Excellence (COE) research. Also, TT acknowledges the support of PPARC.

REFERENCES

- Afonso J., Mobasher B., Chan B., Cram L. 2001, *ApJ*, 559, L101
- Alexander D.M., Bauer F.E., Brandt W.N., Hornschemeier A.E., Vignali C., Garmire G.P., Schneider D.P., Chartas G., Gallagher S.C. 2003, *AJ*, 125, 383
- Arimoto N., Yoshii Y. 1986, *A&A*, 164, 260
- Arimoto N., Yoshii Y., Takahara F. 1992, *A&A*, 253, 21
- Baugh C.M., Cole S., Frenk C.S. 1996 *MNRAS*, 282, 27
- Bautz M.W., Malm M.R., Baganoff F.K., Ricker G.R., Canizares C.R., Brandt W.N., Hornschemeier A.E., Garmire G.P. 2000, *ApJ*, 543, L119
- Bender R., Burstein D., Faber S.M. 1992, *ApJ*, 399, 462
- Benson A.J., Frenk C.S., Baugh C.M., Cole S., Lacey C.G. 2001, *MNRAS*, 327, 1041
- Berger E., Diercks A., Frail D.A., Kulkarni S.R., Bloom J.S., Sari R., Halpern J., Mirabal N. 2001, *ApJ*, 556, 556
- Berger E., Cowie L.L., Kulkarni S.R., Frail D.A., Aussel H., Barger A.J. 2003, *ApJ*, 588, 99
- Binney J. 2004, *MNRAS*, 347, 1093
- Bower R.G., Lucy J.R., Ellis R.S. 1992, *MNRAS*, 254, 601
- Bower R.G., Morris S.L., Bacon R., Wilman R.J., Sullivan M., S. Chapman, Davies R.L., de Zeeuw P.T., Emsellem E. 2004, *astro-ph/0402456*
- Chapman S.C., Smail I., Ivison R.J., Blain A.W. 2002, *MNRAS*, 335, L17
- Chapman S.C., Blain A.W., Ivison R.J., Smail I.R. 2003a, *Nature*, 422, 695
- Chapman S.C., Windhorst R., Odewahn S., Conselice H.Y.C. 2003b, *astro-ph/0308197*
- Chapman S.C., Scott D., Windhorst R.A., Frayer D.T., Borys C., Lewis G.F., Ivison R.J. 2003c, *astro-ph/0310670*
- Clements D.L., Eales S., Wojciechowski K., Webb T.M.A., Lilly S.J., Dunne L., Ivison R.J., McCracken H. et al. 2003, *astro-ph/0312269*
- Combes F., Boissé P., Mazure A., & Blanchard A. 1995, in *Galaxies and Cosmology* (Berlin: Springer-Verlag), 96 (Translated by M. Seymour)
- Cole S., Lacey C.G., Baugh C.M., Frenk C.S. 2000, *MNRAS*, 319, 168
- Dey A., Graham J.R., Ivison R.J., Smail I., Wright G.S., Liu M.C. 1999, *ApJ*, 519, 610
- Diaferio A., Kauffmann G., Balogh M.L., White S.D.M., Schade D., Elligson E. 2001, *MNRAS*, 323, 999
- Djorgovski S., Davis M. 1987, *ApJ*, 313, 59
- Downes D., Solomon P.M. 2003, *ApJ*, 582, 37
- Dressler A., Lynden-Bell D., Burstein D., Davies R.L., Faber S.M., Terlevich R., Wegner G. 1987, *ApJ*, 313, 42
- Dunlop J.S., McLure R.J., Yamada T., Kajisawa M., Peacock J.A., Mann R.G., Hughes D.H., Aretxaga I. et al. 2002, *astro-ph/0205480*
- Eales S., Lilly S., Gear W., Dunne L., Bond J.R., Hammer F., Le Fevre O., Crampton D. 1999, *ApJ*, 515, 518
- Elbaz D., Flores H., Chanial P., Mirabel I.F., Sanders D., P.-A. Duc, Cesarsky C.J., Aussel H. 2002, *A&A*, 381, L1
- Flores H., Hammer F., Desert F.X., Cesarsky C., Thuan T., Crampton D., Eales S., Le Fevre O. et al. 1999a, *A&A*, 343, 389
- Flores H., Hammer F., Thuan T.X., Cesarsky C., Desert F.X., Omont A., Lilly S., Eales S. et al. 1999b, *ApJ*, 517, 148
- Fox M.J., Efstathiou A., Rowan-Robinson M., Dunlop J.S., Scott S., Serjeant S., Mann R.G., Oliver S. et al. 2002, *MNRAS*, 331, 819
- Frayer D.T., Ivison R.J., Scoville N., Evans A.S., Yun M., Smail I., Blain A.W., Kneib J.-P. 1998, *ApJ*, 506, L7
- Frayer D.T., Ivison R.J., Scoville N.Z., Evans A.S., Yun M.S., Smail I., Barger A.J., Blain A.W., Kneib J.-P. 1999, *ApJ*, 514, L13
- Frail D.A., Bertoldi F., Moriarty-Schieven G.H., Berger E., Price P.A., Bloom J.S., Sari R., Kulkarni S.R. et al. 2002, *ApJ*, 565, 829
- Gear W.K., Lilly S.J., Stevens J.A., Clements D.L., Webb T.M., Eales S.A., Dunne L. 2000, *MNRAS*, 316, L51
- Genzel R., Baker A.J., Tacconi L.J., Lutz D., Cox P., Guilleaume S., Omont A. 2003, *ApJ*, 584, 633
- Georgakakis A., Mobasher B., Cram L., Hopkins A., Lidman C., Rowan-Robinson M. 1999, *MNRAS*, 306, 708
- Fabian A.C. et al. 2000, *MNRAS*, 315, L8
- Hughes D.H., Serjeant S., Dunlop J., Rowan-Robinson M., Blain A., Mann R.G., Ivison R., Peacock J. et al. 1998, *Nature*, 394, 241
- Ivison R.J., Smail I., Le Borgne J.-F., Blain A.W., Kneib J.-P., Bezecourt J., Kerr T.H., Davies J.K. 1998, *MNRAS*, 298, 583
- Ivison R.J., Smail I., Frayer D.T., Kneib J.-P., Blain A.W. 2001, *ApJ*, 561, L45
- Ivison R.J., Greve T.R., Smail I., Dunlop J.S., Roche N.D., Scott S.E., Page M.J., Stevens J.A. et al. 2002, *MNRAS*, 337, 1
- Kauffmann G., Charlot S., White S.D.M. 1996, *MNRAS*, 283, L117
- Keel W.C., Wu W., Waddington I., Windhorst R.A., Pascarella S.M. 2002, *AJ*, 123, 3041
- Kodama T., Arimoto N. 1997, *A&A*, 320, 41
- Kodama T., Arimoto N., Barger A.J., Aragon-Salamanca A. 1998, *A&A*, 334, 99
- Lilly S.J., Eales S.A., Gear W.K., Hammer F., Le Fevre O., Crampton D., Bond J.R., Dunne L. 1999, *ApJ*, 518, 641
- Marinoni C., Monaco P., Giuricin G., Costantini B. 1999, *ApJ*, 521, 50
- Massey P., Johnson K.E., Degioia-Eastwood K. 1995, *ApJ*, 454, 151
- Matsushita K., Makishima K., Ikebe Y., Rokutanda E., Yamasaki N.Y., Ohashi T. 1998, *ApJ*, 499, L13
- Neri R., Genzel R., Ivison R.J., Bertoldi F., Blain A.W., Chapman S.C., Cox P., Greve T.R. et al. 2003, *astro-ph/0307310*
- Pierre M., Lidman C., Hunstead R., Alloin D., Casali M., Cesarsky C., Chanial P., Duc P.-A. et al. 2001, *A&A*, 372, L45
- Piro L., Frail D.A., Gorosabel J., Garmire G., Soffitta P., Amati L., Andersen M.I., Antonelli L.A. et al. 2002, *ApJ*, 577, 680
- Scott S.E., Fox M.J., Dunlop J.S., Serjeant S., Peacock J.A., Ivison R.J., Oliver S., Mann R.G. et al. 2002, *MNRAS*, 331, 817
- Sato Y., Cowie L.L., Kawara K., Taniguchi Y., Sofue Y., Matsuhara H., Okuda H. et al. 2002, *ApJ*, 578, L23
- Sato Y., Cowie L.L., Kawara K., Matsuhara H., Okuda H., Sanders D.B., Sofue Y., Taniguchi Y. et al. 2004, *AJ*, 127, 1285
- Serjeant S., Dunlop J.S., Mann R.G., Rowan-Robinson M., Hughes D., Efstathiou A., Blain A., Fox M. et al. 2003, *MNRAS*, 344, 887
- Smail I., Ivison R.J., Blain A.W. 1997, *ApJ*, 490, L5
- Smail I., Ivison R.J., Blain A.W., Kneib J.-P. 2002, *MNRAS*, 331, 495
- Smail I., Ivison R.J., Gilbank D.G., Dunlop J.S., Keel W.C., Motohara K., Stevens J.A. 2003, *ApJ*, 583, 551
- Smith G.P., Treu T., Ellis R., Smail I., Kneib J.-P., Frye B.L. 2001, *ApJ*, 562, 635
- Stanford S.A., Eisenhardt P.R., Dickinson M. 1998, *ApJ*, 492, 461
- Steidel C.C., Adelberger K.L., Shapley A.E., Pettini M., Dickinson M., Giavalisco M. 2000, *ApJ*, 532, 170
- Soucail G., Kneib J.P., Bezecourt J., Metcalfe L., Altieri B., Le Borgne J.F. 1999, *A&A*, 343, L70
- Springel V., White S.D.M., Tormen G., Kauffmann G. 2001, *MNRAS*, 328, 726
- Takagi T., Arimoto N., Hanami H. 2003a, *MNRAS*, 340, 813 [TAH03]
- Takagi T., Vansevicius V., Arimoto N. 2003b, *PASJ*, 55, 385
- Trinchieri G., Fabbiano G., Canizares C.R. 1986, *ApJ*, 310, 637

- Vazdekis A., Arimoto N. 1999, ApJ, 525, 144
- Waskett T.J., Eales S.A., Gear W.K., Puchnarewicz E.M., Lilly S., Flores H., Webb T., Clements D. et al. 2003, MNRAS, 341, 1217
- Webb T.M.A., Lilly S.J., Clements D.L., Eales S., Yun M., Brodwin M., Dunne L., Gear W.K. 2003, ApJ, 597, 680
- Worthey G. 1994, ApJS, 95, 107
- Yamada Y., Arimoto N., Vazdekis A., Pelytier R. 2004, in preparation
- Yoshii Y., Arimoto N. 1987, A&A, 188, 13

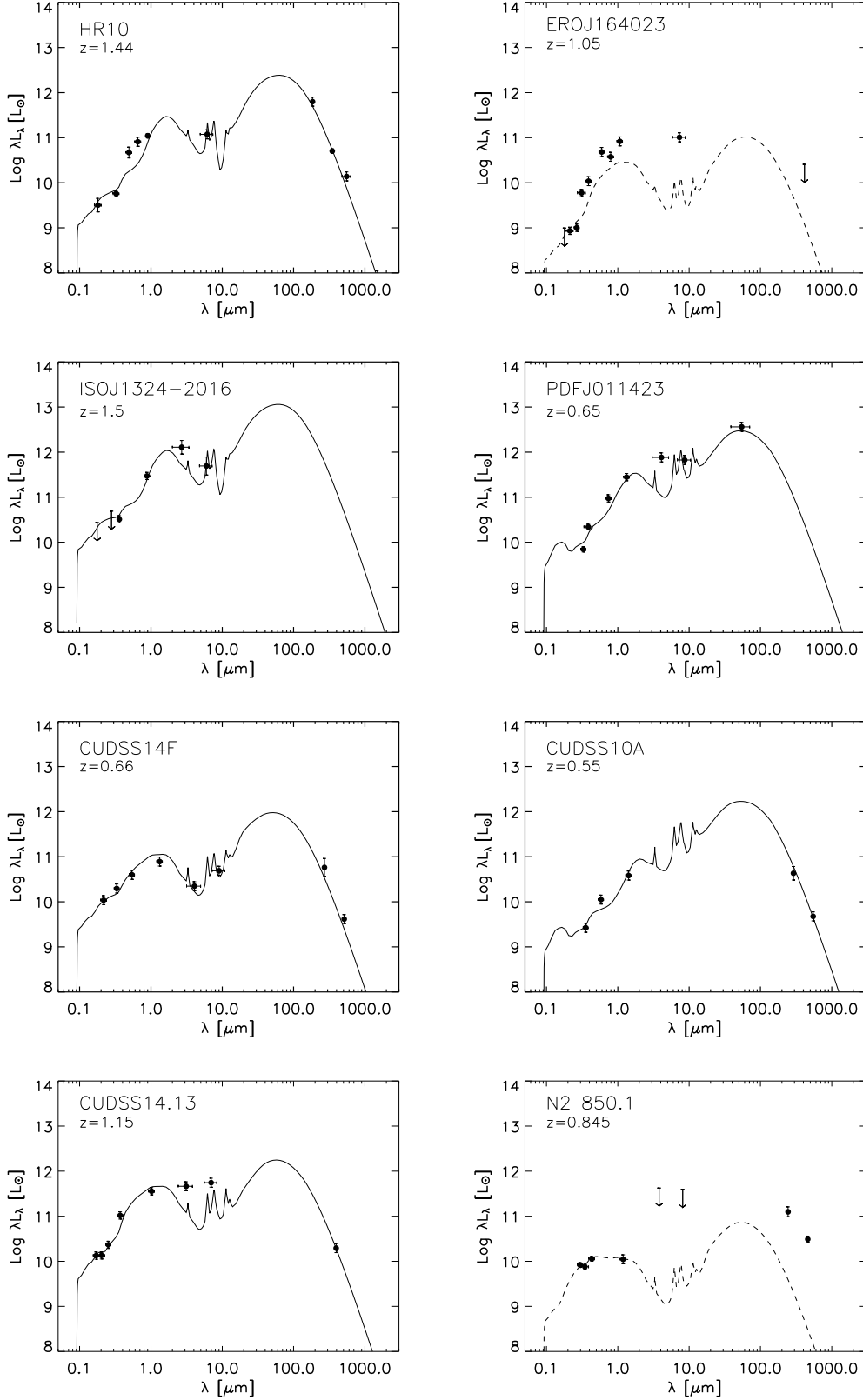


Figure 1. Results of SED fitting with the IMF of $x = 1.10$ in the rest frame. The references for data are given in Table 1. Galaxies for which the SED model is indicated with dashed line are unused in the following analysis (Section 4 and 5).

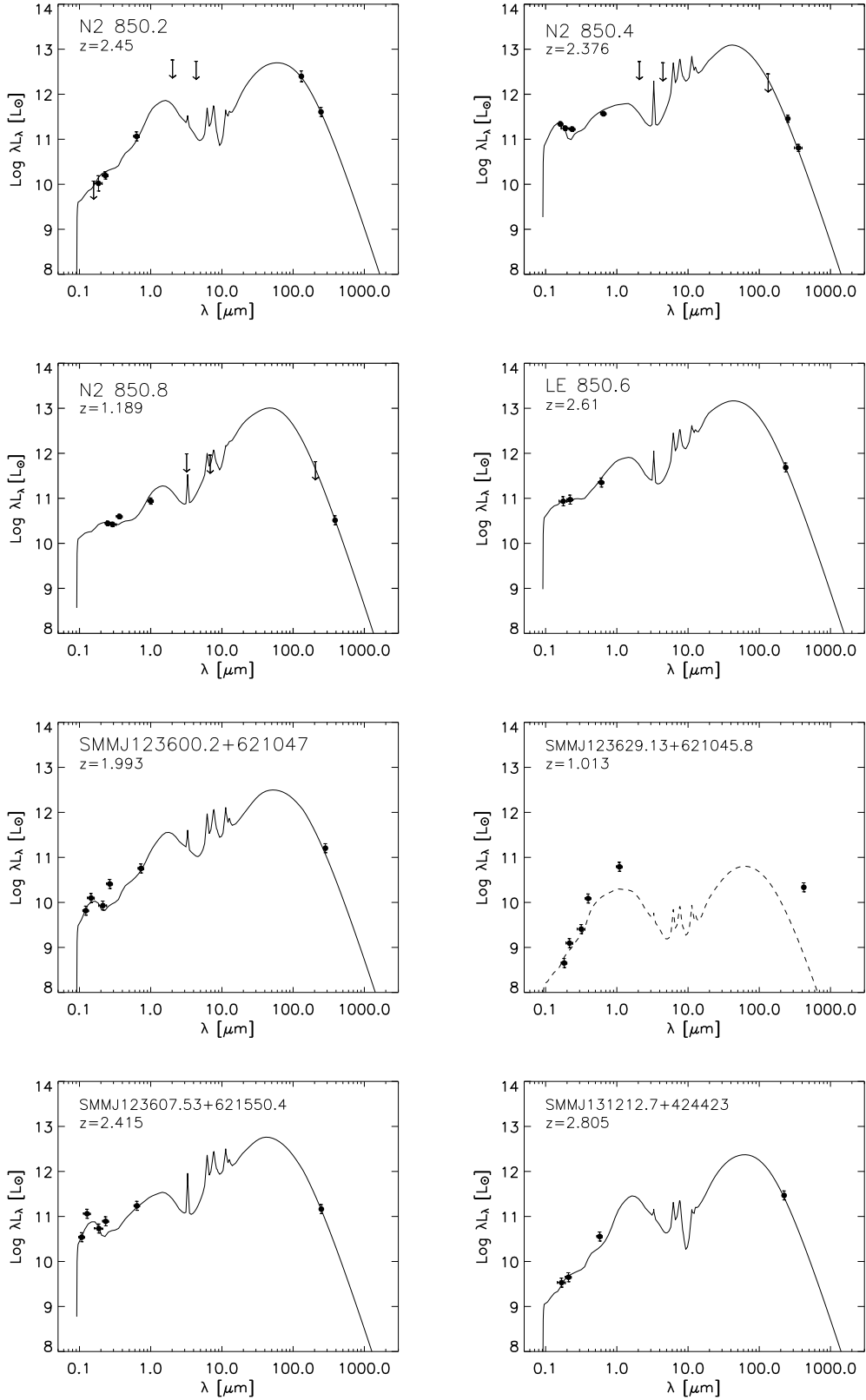


Figure 1. - continued.

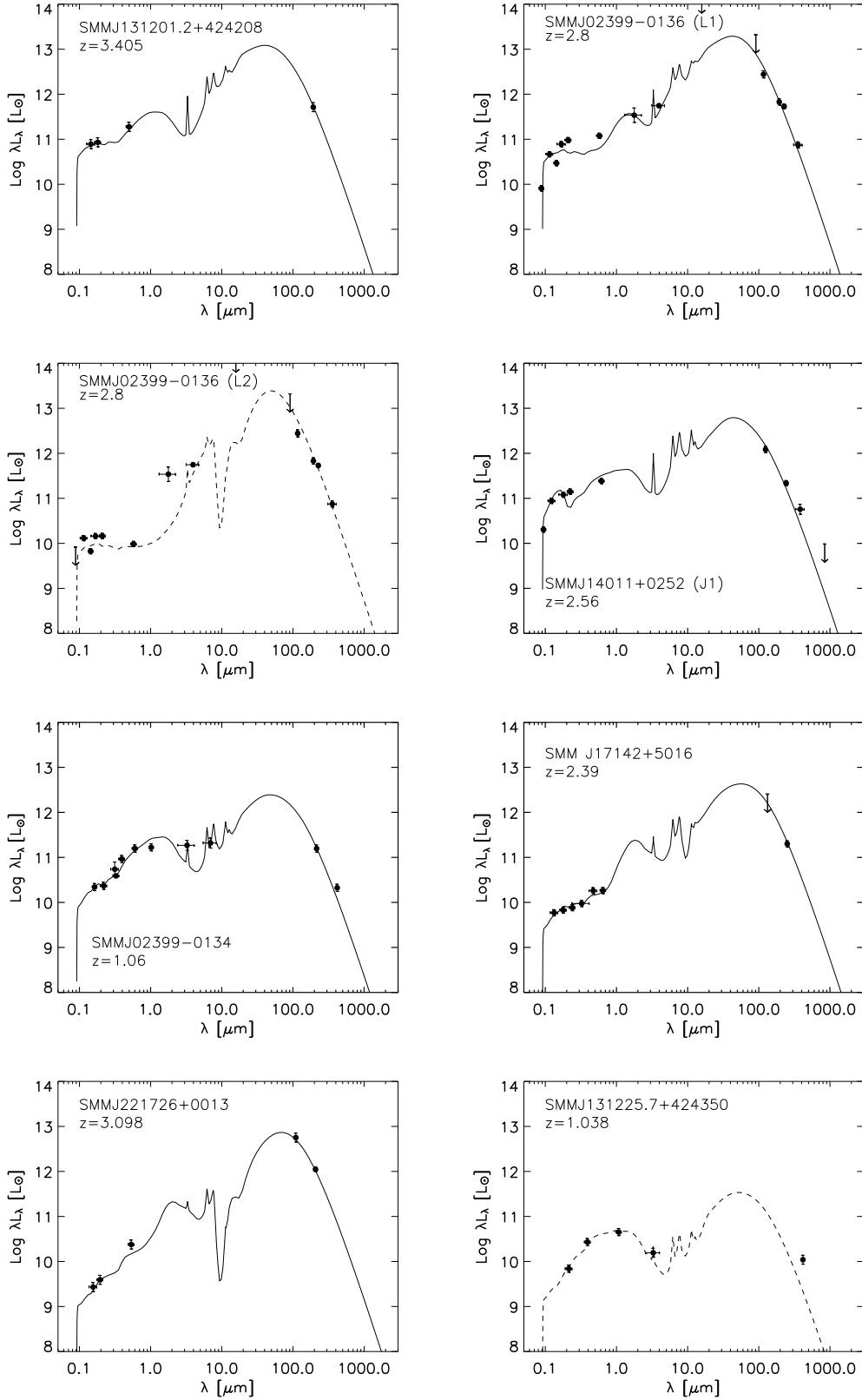


Figure 1. - *continued.*

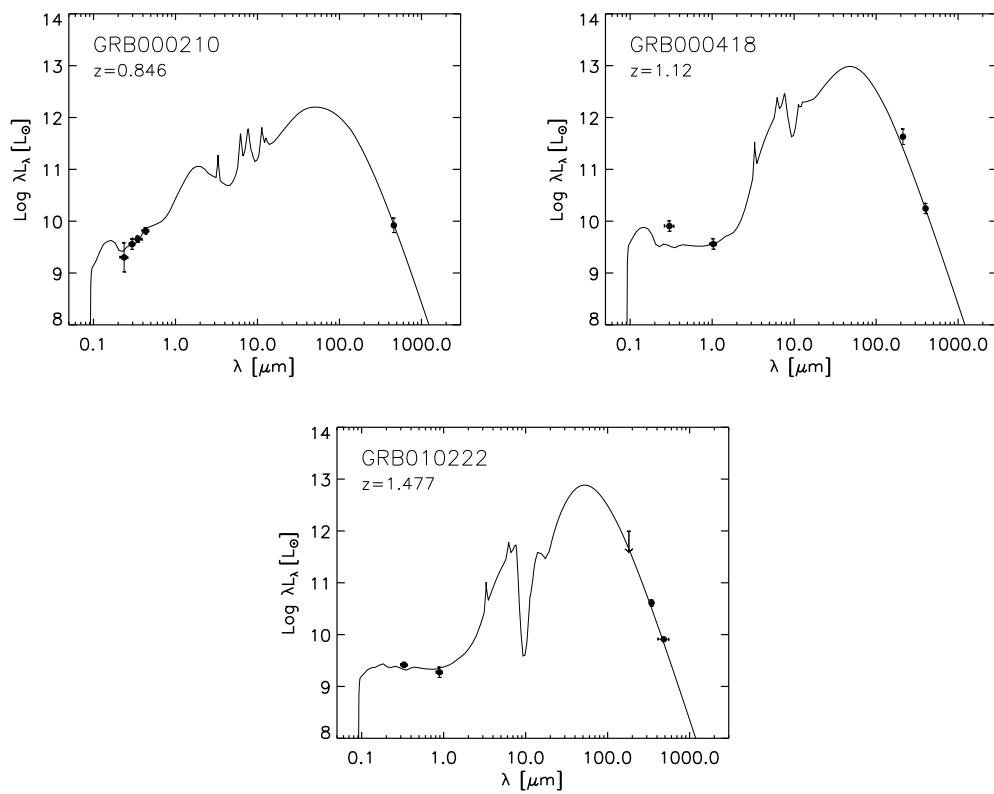


Figure 1. - *continued.*

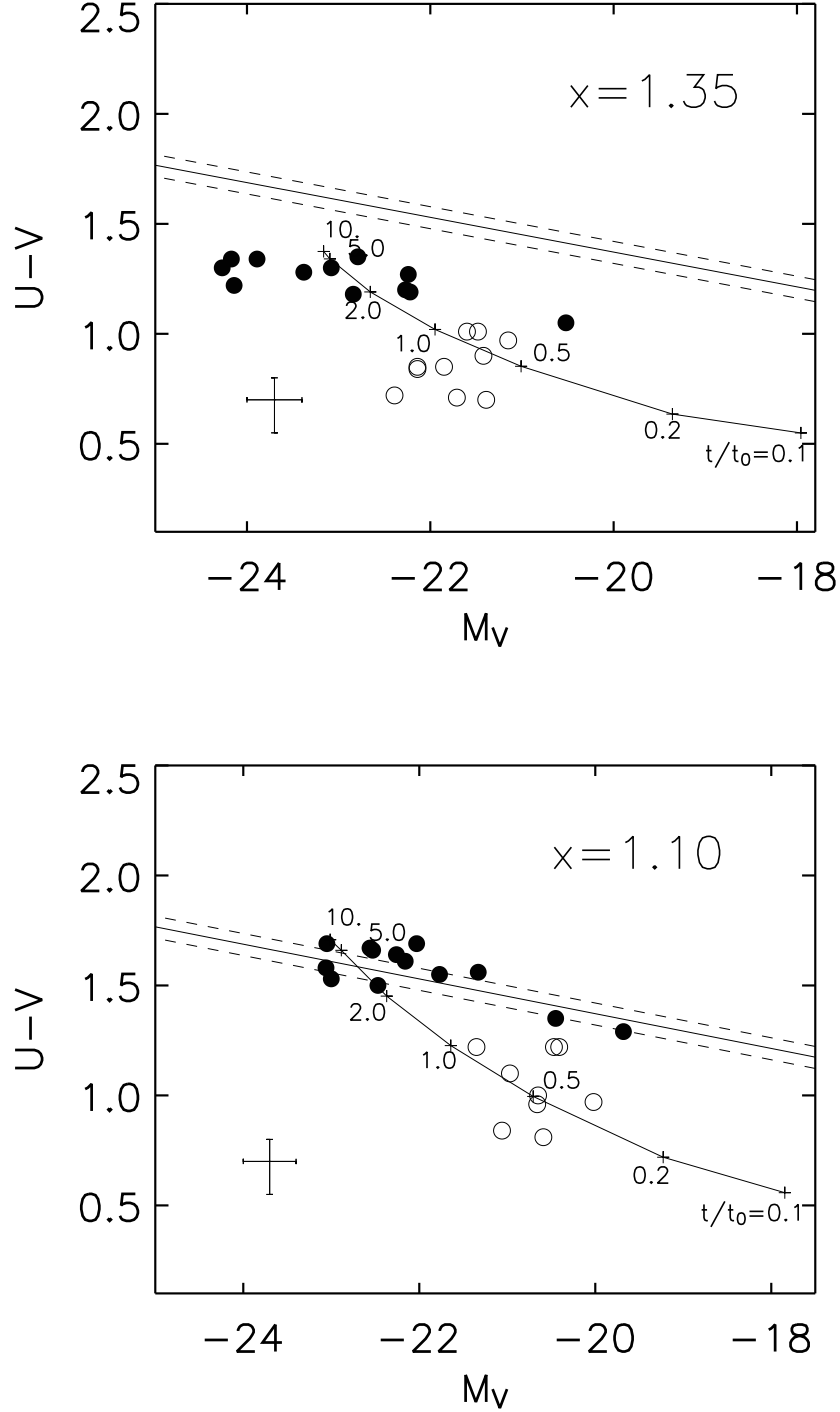


Figure 2. The predicted colours and magnitudes of submm galaxies at the present epoch. Open and solid circles indicate the sample galaxies with age of $t/t_0 \leq 1.0$ and those old than $t/t_0 > 1.0$, respectively. The solid straight line is for the regression line to the CM relation observed in the Coma cluster derived by Bower, Lucey & Ellis (1992), and dashed lines indicate the observed scatter ± 0.05 mag. The depicted loci with starburst age indicate the colours and magnitudes of starburst galaxies formed at $z \sim 3$ with the mass of gas reservoir $M_T = 10^{12} M_\odot$, in which the star formation ceases at indicated starburst age. Note that a starburst galaxy with $M_T = 10^{12} M_\odot$ becomes passively evolving galaxies with $M_V = -23$, i.e., typical brightest elliptical galaxy when $x = 1.10$ and the star formation ceases at the starburst age of $t/t_0 = 5.0$. We show the typical errors at the lower left corner.

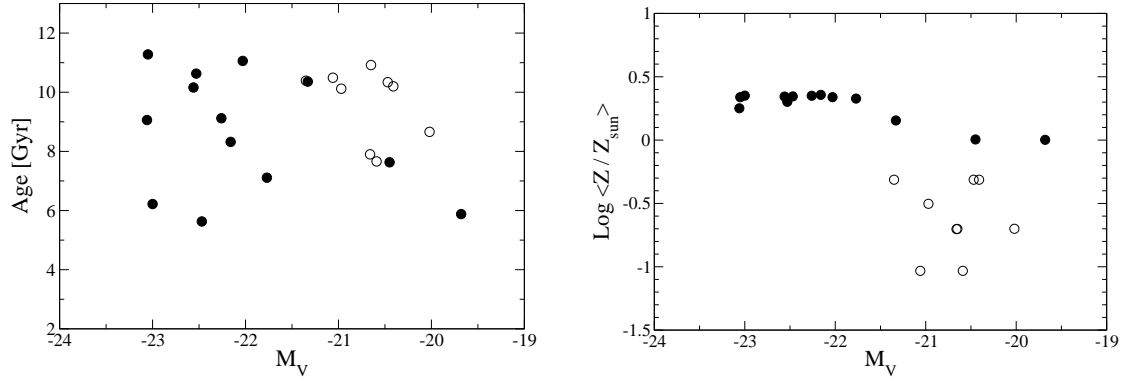


Figure 3. The present-day age and luminosity-weighted stellar metallicity of submm galaxies. The symbols are the same as those in Figure 2. The IMF of $x = 1.10$ is adopted. Left-hand panel: the present-day ages are plotted as a function of present-day M_V . The present-day ages are calculated from the look-back time plus the starburst age assuming $t_0 = 100$ Myr; right-hand panel: the luminosity-weighted stellar metallicities are plotted as a function of present-day M_V .

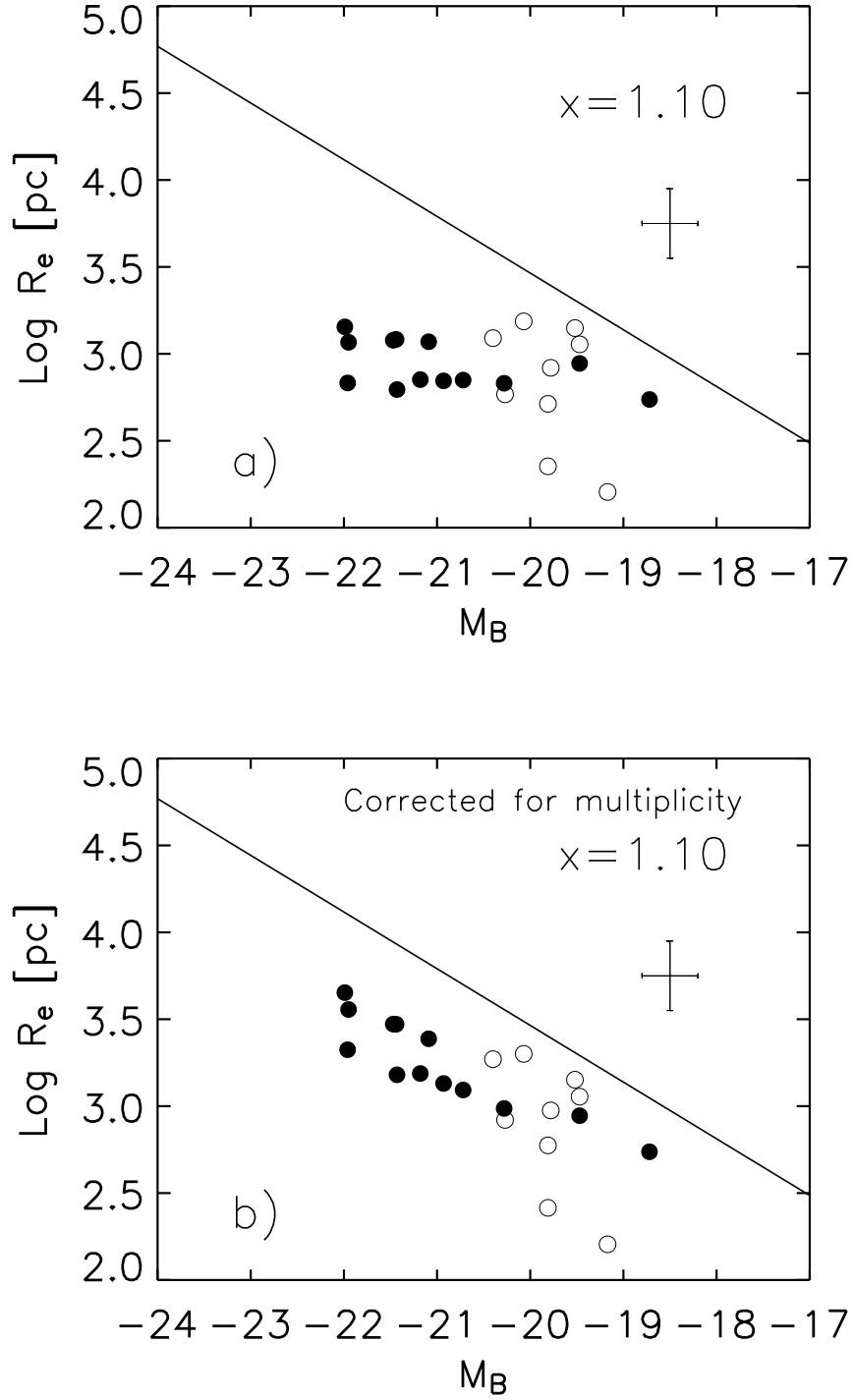


Figure 4. a) Comparison of B -band magnitudes and effective radii with the observed size-magnitude relation of elliptical galaxies (solid line) obtained from the sample of Bender et al. (1992). The symbols are the same as those in Figure 2. The typical errors are shown. b) Same as a), but corrected for the multiplicity (see text in detail).

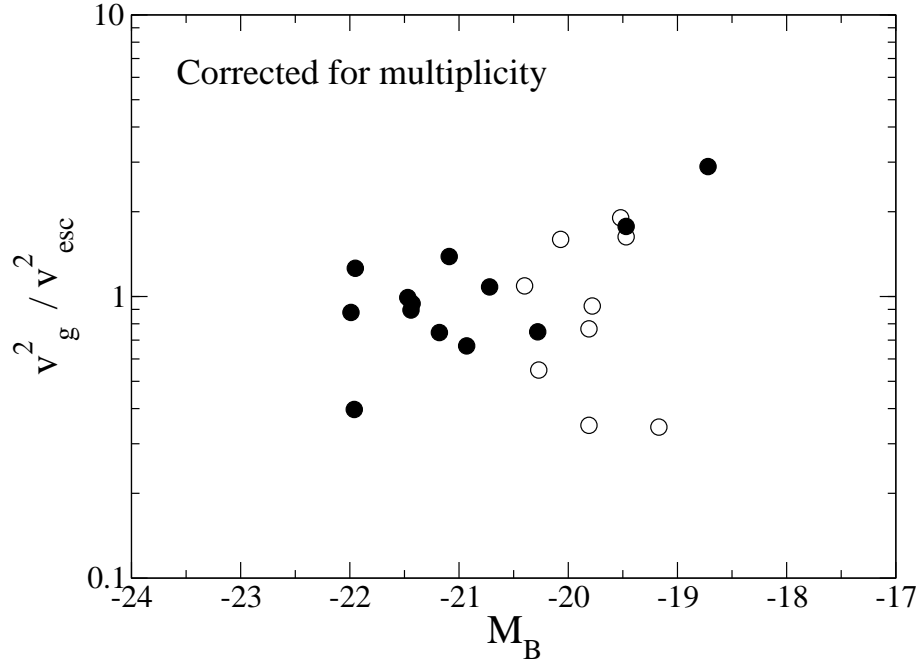


Figure 5. The comparison of the gas velocity by feedback with the escape velocity as a function of the present-day B magnitude with the IMF of $x = 1.10$. The symbols are the same as those in Figure 2. The squared velocity ratio is corrected for the multiplicity. See text in detail.

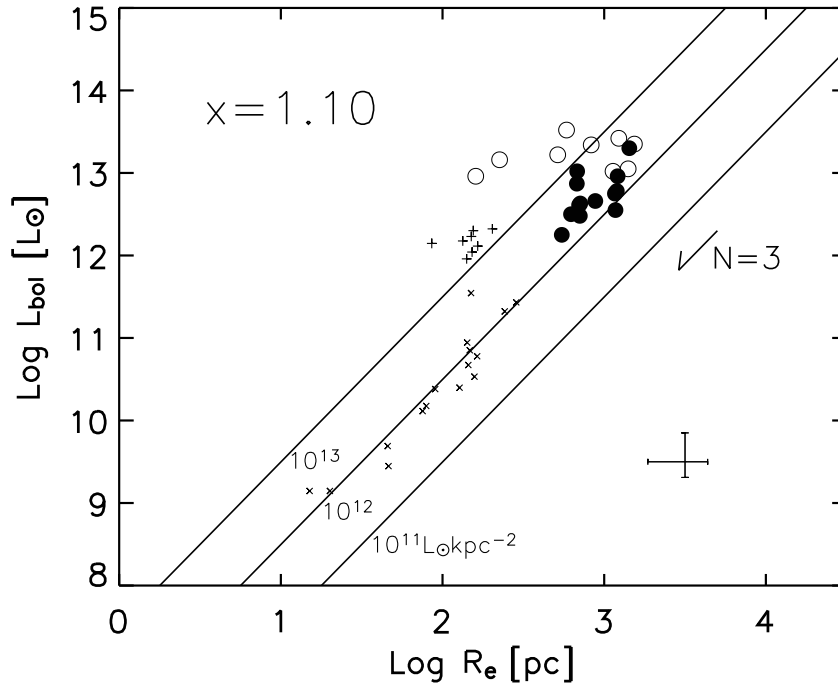


Figure 6. The bolometric luminosities of the sample galaxies plotted against intrinsic effective radii derived from the SED fitting. Crosses (\times) and pluses ($+$) indicate UVSBGs and ULIRGs, taken from TAH03. The other symbols are the same as those in Figure 2. We indicate the correction factor for the multiplicity with an arrow for the case of $N = 3$. The typical errors are shown.

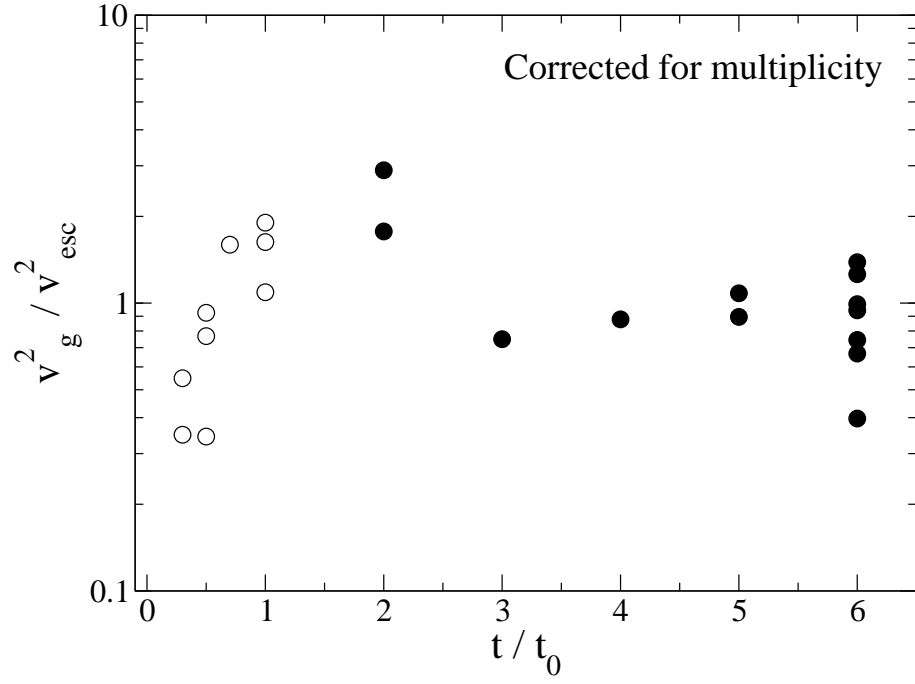


Figure 7. The squared velocity ratio as a function of the starburst age with the IMF of $x = 1.10$. The symbols are the same as those in Figure 2. The squared velocity ratio is corrected for the multiplicity. See text in detail.

Table 1. Summary of observations of the sample

name	z	Amp. ^a	U [μ Jy]	B [μ Jy]	V [μ Jy]	R [μ Jy]	I [μ Jy]	J [μ Jy]	H [μ Jy]	K [μ Jy]	$S_{6.75\mu\text{m}}$ [mJy]	$S_{15\mu\text{m}}$ [mJy]	$S_{450\mu\text{m}}$ [mJy]	$S_{850\mu\text{m}}$ [mJy]	$S_{1.2-1.35\text{mm}}^b$ [mJy]	Ref.
HR10 ^c	1.44	0.16	0.52 ^d	6.4	14.8	27.7	...	0.203	32.3	4.89	2.13 ^e	1, 2
EROJ164023	1.05	1.4	<0.10	0.13	0.19	1.32 ^f	3.00	20.4	21.3	63.0	...	0.530	...	<6	...	3
ISOJ1324-2016	1.50	<0.98	...	<2.8	3.0	67.	0.89	0.76	4
PDFJ011423 ^g	0.65	3.02	11.1	...	91.4	...	485.	4.1	7.6	5, 6
CUDSS14F	0.660	...	3.01	...	8.32	...	27.5	132.	0.115	0.562	20.	2.7	...	7, 8
CUDSS10A	0.550	1.74	...	12.0	100.	23.	4.8	...	7, 8
CUDSS14.13	1.15	...	0.97	1.2	2.5	...	16.4	155.	0.613	1.653	...	3.3	...	9, 10, 11, 12
N2 850.1	0.845	1.92	3.86	2.06	10.3	<1	<2	23.	11.2	...	13, 14
N2 850.2	2.45	<0.16	0.39	0.21	7.9	<1	<2	35.	10.7	...	13, 14, 15
N2 850.4	2.376	3.99	4.48	3.75	27.2	<1	<2	<34.	8.2	2.59 ^h	13, 14, 16
N2 850.8	1.189	2.78	5.79	3.09	35.2	<1	<2	<43.	5.1	...	13, 14, 16
LE 850.6 ⁱ	2.61	2.0	13.1	11.	...	13, 15
SMMJ123600.2+621047	1.993	...	0.12	0.28	...	0.28	1.0	6.4	7.0	...	15, 17
SMMJ123629.13+621045.8	1.013	...	0.045	0.15	...	0.44	2.6	36.8	5.0	...	15
SMMJ123607.53+621550.4	2.415	...	0.41	1.6	...	1.1	2.0	12.2	4.0	...	15
SMMJ131212.7+424423	2.805	0.048	0.080	1.8	5.6	...	15, 17
SMMJ131201.2+424208	3.405	0.70	0.96	5.8	6.2	...	15, 17
SMMJ02399-0136 ^j L1	2.80	2.5	0.153 ^k	1.14	0.905	2.79	4.28	14.7	0.13	0.47	69.	26.0	5.7 ^e	18, 19
SMMJ02399-0136 ^j L2	2.80	2.5	<0.12 ^k	0.320	0.205	0.518	0.653	1.19	0.13	0.47	69.	26.0	5.7 ^e	18, 19
SMMJ14011+0252 J1 ^l	2.56	2.8	0.531	3.00	...	6.00	8.77	41.5	42.	14.6	6.06 ^e	20
SMMJ02399-0134 ^m	1.06	2.5	4.45 ⁿ	6.36	...	21.3	45.	118.	...	212.	0.750	1.80	42.	11.0	...	19, 21
SMMJ17142+5016	2.39	0.0875 ^d	0.135 ^d	...	0.205 ^d	0.343 ^o	0.956 ^o	1.33	5.6	...	22, 23
SMMJ221726+0013	3.098	0.031	0.055	0.92	45.	17.	...	15, 24
SMMJ131225.7+424350	1.038	0.77	5.5	27.	0.027	2.4	...	25
GRB000210	0.846	0.370	0.833	1.22	2.20	3.0	...	26, 27
GRB000418	1.119	1.1	1.7	41.	3.2	...	27, 28
GRB010222	1.477	0.228 ^d	0.445 ^p	<37.8	3.74	1.05 ^h	29

Notes: (a) Amplification by gravitational lens. Flux densities in this table have not been corrected for gravitational amplifications (b) Flux at millimetre wavelength, obtained with JCMT/SCUBA (1.35 mm) or IRAM/MAMBO (1.2 mm) (c) Additional photometry: $S_{12\mu\text{m}}=0.85$ mJy and $S_{3.6\text{cm}}=35$ μ Jy (d) Photometry with *HST*/WFPC2: F300W for U , F450W for B , F606W for V , F814W for I (e) Observed with JCMT/SCUBA at 1.35 mm (f) Originally taken with F702W band of *HST*/WFPC2 (g) Additional photometry: $S_{90\mu\text{m}}=260$ mJy (h) Observed with IRAM/MAMBO at 1.2 mm (i) Additional photometry at R -band (S. Chapman 2004, private communication) (j) Additional photometry: $S_{350\mu\text{m}} < 323$ mJy, $S_{750\mu\text{m}}=28$ mJy (k) Originally taken with F336W band of *HST*/WFPC2 (l) Additional photometry: $S_{3\text{cm}} < 1.8$ mJy (m) Additional photometry: $S_{0.675\mu\text{m}}=15.8$ μ Jy (n) F336W band of *HST*/WFPC2 (o) Photometry with *HST*/NICMOS: F110W for J , F160W for H (p) This flux is contaminated to some extent by the afterglow

REFERENCES. – (1) Dey et al. 1999 (2) Elbaz et al. 2002 (3) Smith et al. 2001 and references therein (4) Pierre et al. 2001 (5) Afonso et al. 2001 (6) Georgakakis et al. 1999 (7) Lilly et al. 1999 (8) Eales et al. 1999 (9) Webb et al. 2003 (10) Clements et al. 2003 (11) Flores et al. 1999a (12) Flores et al. 1999b (13) Ivison et al. 2002 (14) Fox et al. 2002 (15) Chapman et al. 2004, private communication (16) Chapman et al. 2003b (17) Chapman et al. 2003a (18) Ivison et al. 1998 (19) Smail et al. 2002 (20) Ivison et al. 2001 (21) Soucail et al. 1999 (22) Smail et al. 2003 (23) Keel et al. 2002 (24) Chapman et al. 2003c (25) Sato et al. 2004 (26) Piro et al. 2002 (27) Berger et al. 2003 (28) Berger et al. 2001 (29) Frail et al. 2002

Table 2a. The results of SED fitting with the IMF of $x = 1.35$

name	t/t_0	Θ	$E.C.^b$	z	$\log M_T^c$ [M_\odot]	τ_V	$\log \text{SFR}$ [$M_\odot \text{ yr}^{-1}$]	$\log M_*$ [M_\odot]	$\log M_D$ [M_\odot]	$\log L_{bol}$ [L_\odot]	$\log R_e^d$ [pc]	M_V^e	M_B^f	$U - V^g$	$t_{z=0}^h$ [Gyr]	$\log(Z_*/Z_\odot)_{z=0}^i$
HR10	5.0	0.3	SMC	1.44	11.94	15.3	2.74	11.91	9.20	12.74	2.76	-23.08	-22.11	1.30	9.0	-0.09
<i>EROJ164023^a</i>	<i>6.0</i>	<i>0.5</i>	<i>MW</i>	<i>1.05</i>	<i>10.94</i>	<i>4.3</i>	<i>1.51</i>	<i>10.93</i>	<i>7.76</i>	<i>11.59</i>	<i>2.49</i>	<i>-20.72</i>	<i>-19.76</i>	<i>1.27</i>	<i>8.0</i>	<i>-0.06</i>
ISOJ1324-2016	5.0	0.3	SMC	1.50	12.42	15.3	3.22	12.39	9.68	13.22	3.00	-24.27	-23.30	1.30	9.2	-0.09
PDFJ011423	6.0	0.3	MW	0.65	12.21	11.9	2.78	12.20	9.03	12.86	2.91	-24.14	-23.20	1.22	6.2	-0.06
CUDSS14F	2.0	0.9	SMC	0.66	10.94	5.2	2.44	10.68	8.47	12.21	2.63	-20.52	-19.64	1.05	5.9	-0.38
CUDSS10A	5.0	0.3	MW	0.55	11.66	18.0	2.47	11.63	8.65	12.45	2.63	-22.84	-21.92	1.18	5.5	-0.10
CUDSS14.13	6.0	0.5	MW	1.15	12.02	4.3	2.58	12.00	8.84	12.67	3.03	-23.38	-22.41	1.28	8.3	-0.06
<i>N2 850.1</i>	<i>0.5</i>	<i>0.4</i>	<i>SMC</i>	<i>0.84</i>	<i>12.07</i>	<i>32.5</i>	<i>3.57</i>	<i>11.00</i>	<i>8.89</i>	<i>13.07</i>	<i>2.43</i>	<i>-21.66</i>	<i>-20.88</i>	<i>0.81</i>	<i>6.6</i>	<i>-1.05</i>
N2 850.2	5.0	0.3	SMC	2.45	12.32	15.3	3.12	12.29	9.58	13.12	2.95	-23.89	-22.90	1.34	10.6	-0.09
N2 850.4	0.5	0.7	LMC	2.38	12.44	8.9	3.93	11.36	9.11	13.44	2.86	-22.14	-21.34	0.84	10.1	-1.05
N2 850.8	0.7	0.7	SMC	1.19	11.87	10.8	3.42	11.03	8.92	13.03	2.69	-21.42	-20.60	0.90	7.9	-0.86
LE 850.6	0.3	0.7	SMC	2.61	12.90	8.9	4.25	11.44	9.25	13.66	2.89	-22.39	-21.66	0.72	10.3	-1.40
SMMJ123600.2+621047	6.0	0.3	MW	1.99	12.40	11.9	2.97	12.39	9.22	13.05	3.00	-24.17	-23.18	1.34	10.2	-0.06
<i>SMMJ123629.13+621045.8^a</i>	<i>6.0</i>	<i>0.5</i>	<i>SMC</i>	<i>1.01</i>	<i>10.50</i>	<i>3.6</i>	<i>1.07</i>	<i>10.49</i>	<i>7.60</i>	<i>11.16</i>	<i>2.27</i>	<i>-19.64</i>	<i>-18.68</i>	<i>1.27</i>	<i>7.8</i>	<i>-0.06</i>
SMMJ123607.53+621550.4	1.0	1.2	MW	2.42	11.80	4.3	3.39	11.19	8.80	13.04	3.00	-21.48	-20.60	1.01	10.2	-0.68
SMMJ131212.7+424423	5.0	0.3	SMC	2.81	11.89	15.3	2.69	11.86	9.15	12.69	2.74	-22.79	-21.80	1.35	11.0	-0.09
SMMJ131201.2+424208	0.5	0.9	LMC	3.40	12.35	5.4	3.84	11.27	9.02	13.35	2.92	-21.85	-21.05	0.85	10.9	-1.05
SMMJ02399-0136 L1	0.5	0.7	LMC	2.80	12.45	8.9	3.94	11.38	9.12	13.45	2.86	-22.14	-21.34	0.85	10.5	-1.05
<i>SMMJ02399-0136 L2^a</i>	<i>0.3</i>	<i>0.3</i>	<i>LMC</i>	<i>2.80</i>	<i>12.69</i>	<i>40.8</i>	<i>4.04</i>	<i>11.23</i>	<i>8.91</i>	<i>13.42</i>	<i>2.42</i>	<i>-21.86</i>	<i>-21.12</i>	<i>0.72</i>	<i>10.5</i>	<i>-1.40</i>
SMMJ14011+0252 J1	1.0	1.4	MW	2.56	11.85	3.2	3.44	11.24	8.86	13.09	3.10	-21.60	-20.73	1.01	10.3	-0.68
SMMJ02399-0134	1.0	1.0	SMC	1.06	11.55	5.3	3.15	10.95	8.83	12.82	2.80	-21.15	-20.30	0.97	7.5	-0.69
SMMJ17142+5016	3.0	0.4	LMC	2.39	11.72	15.7	3.01	11.60	9.10	12.85	2.73	-22.24	-21.28	1.27	10.4	-0.23
SMMJ221726+0013	2.0	0.3	SMC	3.10	11.84	46.7	3.33	11.58	9.37	13.09	2.60	-22.22	-21.28	1.19	10.9	-0.37
<i>SMMJ131225.7+424350^a</i>	<i>3.0</i>	<i>1.0</i>	<i>LMC</i>	<i>1.04</i>	<i>10.62</i>	<i>2.5</i>	<i>1.91</i>	<i>10.50</i>	<i>7.99</i>	<i>11.75</i>	<i>2.58</i>	<i>-19.74</i>	<i>-18.81</i>	<i>1.18</i>	<i>7.7</i>	<i>-0.23</i>
GRB000210	4.0	0.3	SMC	0.85	11.55	22.9	2.60	11.49	8.96	12.51	2.55	-22.27	-21.33	1.20	7.0	-0.15
GRB000418	0.3	0.3	MW	1.12	12.51	57.3	3.86	11.05	8.59	13.22	2.33	-21.71	-20.98	0.71	7.7	-1.39
GRB010222	0.3	0.3	MW	1.48	12.44	57.3	3.79	10.98	8.52	13.15	2.30	-21.39	-20.66	0.70	8.6	-1.40

Notes: (a) Submm galaxies unused in Section 4 and 5 (b) extinction curve (c) initial mass of gas reservoir (d) intrinsic effective radius (e) present-day V -band absolute magnitude of submm galaxies (f) present-day B -band absolute magnitude of submm galaxies (g) present-day $U - V$ of submm galaxies (h) age of submm galaxies at $z = 0$ when $t_0=100$ Myr (i) mean luminosity-weighted metallicity of stars

Table 2b. The results of SED fitting with the IMF of $x = 1.10$

name	t/t_0	Θ	$E.C^b$	z^c	$\log M_T^d$ [M_\odot]	τ_V	$\log \text{SFR}$ [$M_\odot \text{ yr}^{-1}$]	$\log M_*$ [M_\odot]	$\log M_D$ [M_\odot]	$\log L_{bol}$ [L_\odot]	$\log R_e^e$ [pc]	M_V^f	M_B^g	$U - V^h$	$t_{z=0}^i$ [Gyr]	$\log(Z_*/Z_\odot)_{z=0}^j$
HR10	6.0	0.5	SMC	1.44	11.67	14.8	2.47	11.64	9.34	12.63	2.85	-22.26	-21.18	1.64	9.1	0.35
<i>EROJ164023^a</i>	<i>6.0</i>	<i>0.9</i>	<i>SMC</i>	<i>1.05</i>	<i>10.36</i>	<i>4.5</i>	<i>1.16</i>	<i>10.34</i>	<i>8.04</i>	<i>11.32</i>	<i>2.45</i>	<i>-19.13</i>	<i>-18.06</i>	<i>1.60</i>	<i>8.0</i>	<i>0.36</i>
ISOJ1324-2016	4.0	0.7	SMC	1.50	12.04	14.5	3.23	11.96	9.95	13.30	3.16	-23.06	-21.99	1.58	9.1	0.25
PDFJ011423	6.0	0.7	MW	0.65	11.81	8.9	2.60	11.78	9.20	12.75	3.07	-23.00	-21.95	1.53	6.2	0.35
CUDSS14F	2.0	1.6	SMC	0.66	10.70	4.8	2.25	10.40	8.65	12.25	2.74	-19.68	-18.72	1.29	5.9	0.00
CUDSS10A	6.0	0.5	MW	0.55	11.56	17.4	2.35	11.53	8.95	12.50	2.79	-22.47	-21.43	1.50	5.6	0.34
CUDSS14.13	6.0	0.9	LMC	1.15	11.60	3.8	2.39	11.57	9.13	12.55	3.07	-22.16	-21.09	1.61	8.3	0.36
<i>N2 850.1^a</i>	<i>2.0</i>	<i>2.4</i>	<i>SMC</i>	<i>0.84</i>	<i>9.60</i>	<i>2.1</i>	<i>1.16</i>	<i>9.31</i>	<i>7.55</i>	<i>11.16</i>	<i>2.37</i>	<i>-16.80</i>	<i>-15.83</i>	<i>1.32</i>	<i>6.8</i>	<i>0.01</i>
N2 850.2	5.0	0.7	SMC	2.45	11.86	10.5	2.85	11.81	9.66	12.96	3.08	-22.53	-21.44	1.66	10.6	0.30
N2 850.4	0.7	2.2	MW	2.38	11.90	3.4	3.47	11.03	9.06	13.35	3.19	-20.97	-20.07	1.10	10.1	-0.50
N2 850.8	0.5	1.0	SMC	1.19	11.87	12.9	3.37	10.76	9.04	13.22	2.71	-20.66	-19.81	0.96	7.9	-0.70
LE 850.6	1.0	1.4	LMC	2.61	11.87	6.1	3.49	11.23	9.40	13.42	3.09	-21.35	-20.40	1.22	10.4	-0.31
SMMJ123600.2+621047	6.0	0.7	MW	1.99	11.83	8.9	2.63	11.80	9.23	12.78	3.08	-22.56	-21.47	1.67	10.2	0.34
<i>SMMJ123629.13+621045.8^a</i>	<i>6.0</i>	<i>1.0</i>	<i>SMC</i>	<i>1.01</i>	<i>10.16</i>	<i>3.7</i>	<i>0.96</i>	<i>10.14</i>	<i>7.84</i>	<i>11.12</i>	<i>2.40</i>	<i>-18.65</i>	<i>-17.58</i>	<i>1.59</i>	<i>7.8</i>	<i>0.37</i>
SMMJ123607.53+621550.4	1.0	2.0	MW	2.42	11.49	4.2	3.11	10.84	8.88	13.02	3.05	-20.41	-19.47	1.22	10.2	-0.31
SMMJ131212.7+424423	6.0	0.5	SMC	2.81	11.66	14.8	2.45	11.63	9.33	12.61	2.84	-22.03	-20.93	1.69	11.1	0.34
SMMJ131201.2+424208	0.5	1.4	LMC	3.40	11.99	5.5	3.49	10.88	9.02	13.34	2.92	-20.65	-19.78	1.00	10.9	-0.70
SMMJ02399-0136 L1	0.3	0.9	LMC	2.80	12.45	11.3	3.81	10.96	9.04	13.52	2.77	-21.06	-20.27	0.84	10.5	-1.03
<i>SMMJ02399-0136 L2^a</i>	<i>0.3</i>	<i>0.4</i>	<i>LMC</i>	<i>2.80</i>	<i>12.43</i>	<i>57.2</i>	<i>3.79</i>	<i>10.94</i>	<i>9.01</i>	<i>13.47</i>	<i>2.40</i>	<i>-21.01</i>	<i>-20.22</i>	<i>0.84</i>	<i>10.5</i>	<i>-1.03</i>
SMMJ14011+0252 J1	1.0	2.4	MW	2.56	11.52	2.9	3.13	10.87	8.91	13.05	3.15	-20.47	-19.52	1.22	10.3	-0.31
SMMJ02399-0134	2.0	1.6	LMC	1.06	11.11	4.0	2.67	10.82	8.92	12.66	2.94	-20.45	-19.47	1.35	7.6	0.01
SMMJ17142+5016	3.0	0.7	LMC	2.39	11.46	16.4	2.85	11.31	9.30	12.87	2.83	-21.33	-20.28	1.56	10.4	0.15
SMMJ221726+0013	6.0	0.3	SMC	3.10	12.08	41.0	2.87	12.05	9.75	13.02	2.83	-23.05	-21.96	1.69	11.3	0.34
<i>SMMJ131225.7+424350^a</i>	<i>2.0</i>	<i>2.0</i>	<i>SMC</i>	<i>1.04</i>	<i>10.26</i>	<i>3.1</i>	<i>1.82</i>	<i>9.97</i>	<i>8.21</i>	<i>11.81</i>	<i>2.62</i>	<i>-18.33</i>	<i>-17.35</i>	<i>1.34</i>	<i>7.6</i>	<i>0.01</i>
GRB000210	5.0	0.7	MW	0.85	11.39	12.4	2.38	11.35	8.92	12.48	2.85	-21.77	-20.72	1.55	7.1	0.33
GRB000418	0.3	0.5	MW	1.12	12.13	51.5	3.49	10.65	8.58	13.16	2.35	-20.59	-19.81	0.81	7.7	-1.03
GRB010222	0.5	0.4	LMC	1.48	11.65	67.8	3.15	10.54	8.68	12.96	2.21	-20.02	-19.17	0.97	8.7	-0.70

See notes in Table 2a

APPENDIX A: SUMMARY OF OBSERVATIONS**A1 Extremely red objects**

We collect extremely red objects (EROs) detected in the MIR – submm wavelengths. In order to increase the sample, we included EROs detected at the MIR wavelengths by Infrared Space Observatory (*ISO*), but not have observed flux at submm wavelengths. The samples are HR10, EROJ164023, ISOJ1324-2016, and PDFJ011423.

These EROs are bright in the NIR enough to perform spectroscopic observations, and therefore redshifts are spectroscopically determined. From the spectra, EROJ164023, ISOJ1324-2016 and PDFJ011423 are suggested to be composite starburst-AGN galaxies (Smith et al. 2001; Pierre et al. 2001; Afonso et al. 2001), while there is no signature of AGN in the spectra of HR10 (Dey et al. 1999).

A2 Submm-selected galaxies*A2.1 Canada-UK Deep Submm Survey*

The secure optical identifications of six submm sources detected in the Canada-UK Deep Submm Survey (CUDSS) are reported in Lilly et al. (1999), one of which is a nearby spiral galaxy at $z = 0.074$ and therefore excluded in this study. Two submm galaxies (CUDSS 14F and 14A) are associated with radio sources. CUDSS 14F is detected with *ISO* at 6.75 and 15 μm , and therefore this source is most securely identified, despite the faintest submm flux among these sample. The redshifts of CUDSS 14F and 10A are already known to be $z = 0.660$ and 0.550 , respectively. So far, no signature of AGN activity is found in these submm galaxies (e.g. Gear et al. 2000).

Together with CUDSS 14F and 10A, we collect CUDSS14.13 from the new catalogue by Webb et al. (2003). The multi-band photometric data are reported in Clements et al. (2003). This source has been detected at X-ray wavelengths (Waskett et al. 2003) and likely contains an AGN.

A2.2 SCUBA 8-mJy survey

The SCUBA 8-mJy survey is the largest submm extragalactic survey undertaken to date, covering 260 arcmin². Ivison et al. (2002) performed the optical identification of these submm galaxies in the Lockman Hole and ELAIS N2 regions by using the 1.4-GHz imaging map; as a result, 18 out of 30 submm sources are reliably identified as radio sources. The spectroscopic redshift of some sources are available in Chapman et al. (2003a) and also provided by S. Chapman (2004, private communication). From this survey, 5 sources (N2 850.1, N2 850.4, N2 850.8, and LE 850.6) satisfies the requirements for our sample. Note that the *R*-band data of LE 850.6 is provided by S. Chapman (2004, private communication).

Although the radio map suggests N2 850.1 is associated with the bright, compact optical galaxy at $z = 0.845$, Ivison et al. (2002) claim that this galaxy acts as a gravitational lens to amplify the background faint submm source, considering the unreasonable 450-/850- μm and submm/radio spectral indices as a submm source at $z < 1$ (see also Chapman et al. 2002). Assuming that the galaxy at $z = 0.845$ is

the true optical counterpart, we fit the SED of this submm source, but found no suitable SED model.

A2.3 Hubble Deep Field and SA13 field

The photometric data and the spectroscopic redshifts of sample in these fields (i.e. SMMJ123600.2+621047, SMMJ123629.13+621045.8, SMM J123607.53+621550.4, SMMJ131212.7+424423, and SMMJ131201.2+424208) are taken from Chapman et al. (2003a) or provided by S. Chapman (2004, private communication) if not available in Chapman et al. (2003a).

The deep SCUBA map of HDF is reported by Dunlop et al. (1998), which is re-analysed by Serjeant et al. (2003). No source is however collected from these reports, since these sources are too faint at submm wavelengths, compared to the other sample. Note that even the optical identification of the brightest source HDF850.1 is complicated by the possible gravitational lensing by a foreground galaxy (Dunlop et al. 2002).

A3 Lensed submm galaxies

The effects of gravitational lens has been used to push below the confusion limit of the blank-field surveys. In the list of submm sources by Smail et al. (2002), three submm sources, SMM J02399-0136, SMM J14011+0252 and SMM J02399-0124 have enough photometric data to perform the SED fitting, all of which have spectroscopic redshifts. We adopt the lens amplification of 2.5, 2.8 and 2.5 for SMM J02399-0136, SMM J14011+0252 and SMM J02399-0134, respectively (Smail et al. 2002).

SMM J02399-0136 is one of the brightest submm sources with the 850- μm flux of 26 mJy. The optical counterpart of SMM J02399-0136 is a system of two interacting/merging galaxies, named L1 for the compact component and L2 for the disturbed relatively diffuse component. The spectroscopic redshifts ($z = 2.80$) measured for each component suggest that L1 component is physically associated with L2 component. The angular separation of L1 and L2 is about 3'' (22 kpc for the adopted cosmology). Each component is resolved by a 1.3'' synthesized beam at 1.4-GHz, and appears to have different radio spectral indices. The UV spectrum of L1 exhibits high-ionization lines with the width of $\sim 1000 \text{ km s}^{-1}$ and therefore this component probably has an AGN in the center. The presence of an AGN is also confirmed by the detection in the hard X-ray by *Chandra* (Bautz et al. 2000). On the other hand, the presence of a large amount of gas ($\text{M}(\text{H}_2) \sim 2 \times 10^{11} \text{ M}_\odot$) is inferred from the strong CO emission lines. This means that a significant fraction of FIR luminosity could arise from starburst activity. The rest-frame FIR-to-5-GHz flux ratio is similar to that seen in nearby starbursts. These observations suggest that SMM J02399-0136 is a system of composite starburst-AGN galaxy.

The optical counterpart of SMM J14011+0252 is again an interacting/merging pair of galaxies at $z = 2.56$, J1 and J2 (Ivison et al. 2001). The CO position by Downes & Solomon (2003) differs significantly ($\gtrsim 1''$) from those obtained by Frayer et al. (1999) and Ivison et al. (2001); as a result, the new position agrees with the optical position

Table 3. Summary of SED fitting results

Age	$x = 1.35$	$x = 1.10$
$t/t_0 \leq 1$	10	10
$t/t_0 = 2$	2	2
$t/t_0 = 3$	1	1
$t/t_0 = 4$	1	1
$t/t_0 = 5$	5	2
$t/t_0 = 6$	3	6
Optical depth		
$\tau_V \leq 3.$	0	1
$3 < \tau_V \leq 5.$	3	3
$5 < \tau_V \leq 10.$	6	4
$10 < \tau_V \leq 20.$	9	9
$\tau_V > 20.$	4	3
Extinction curve		
MW	8	8
LMC	4	7
SMC	10	7

Note: we exclude EROJ164023, N2 850.1, SMMJ123629.13+621045.8, and SMMJ131225.7+424350, for which we find no reasonable SED fit.

 Table 4. The mean characteristics of old submm galaxies at $z = 0$.

	Sample	$\langle z \rangle$	$\langle M_V \rangle$	$\langle U - V \rangle$	$\langle t_{z=0} \rangle$ [Gyr]	$\langle \log(Z_*/Z_\odot) \rangle$
Bright sample ($M_V < -22$)	9	1.7	-22.57	1.62	9.0 (9.0) ^a	0.33
Faint sample ($M_V > -22$)	4	1.2	-20.81	1.44	7.7 (9.0) ^a	0.14
All sample	13	1.6	-22.03	1.56	8.64	0.27

Note: the mean values are given for old submm galaxies ($t/t_0 \geq 2$). All the values are derived with the IMF of $x = 1.10$. a) The mean of present-day age including young submm galaxies.

of the J1 complex within the 1σ errors³. The high resolution image with the HST shows that the morphology of J1 component is complex; i.e. main component with relatively regular shape is associated with an extended envelope. Interestingly enough, the CO and dust emission is spatially extended over few arcseconds ($\gtrsim 10$ kpc). Therefore, this galaxy is powered by starbursts rather than an AGN, which is consistent with the spectral features at rest-frame 1200 – 2400 Å (Ivison et al. 2000). Also, this system is undetected in hard X-ray observations with *Chandra* (Fabian et al. 2000).

SMM J02399-0134 is identified with a ring galaxy at $z = 1.06$, which is also relatively bright at 7 and 15 μm (Soucail et al. 1999). The emission lines [OII] 3727 Å and [NeV] 3426 Å are detected, which are typical of starburst galaxies hosting a central AGN (Soucail et al. 1999). The

presence of an obscured AGN is confirmed through a detection in the hard X-ray band by *Chandra* (Bautz et al. 2000).

A4 Submm galaxies in the proto-cluster region

If submm sources at high redshifts are progenitors of present-day elliptical galaxies, they should be found preferentially in over-density regions at high redshifts, i.e. in proto-clusters.

Smail et al. (2003) report the spectroscopically confirmed, submm-selected companion to a high- z radio galaxy 53W002 which has been shown to reside in an over-density of Ly- α detected galaxies. By using a 1.4-GHz map, this submm source, SMM J17142+5016, is identified with a narrow-line AGN at $z = 2.390$. This galaxy itself is one of the brightest Ly- α emitters in this region, and associated with an extended ($> 6''$) Ly- α halo.

SMMJ221726+0013 is a bright submm galaxy resides in a giant Ly- α halo (Chapman et al. 2003c) at $z = 3.098$. This giant Ly- α halo ‘blob-1’ ($\gtrsim 100$ kpc) lies in an over-density region discovered in the survey of Lyman-break galaxies (Steidel et al. 2000). Chapman et al. (2003c) identify the optical counterpart as an elongated galaxy J1. The optical-NIR photometric data of J1 are provided by S. Chapman (2004,

³ Downes and Solomon (2002) also suggest that SMM J14011+0252 is gravitationally lensed not only by the foreground cluster, but also by an individual galaxy on the line of sight. Since this hypothesis is not yet confirmed well (e.g. the redshift of suspected lensing galaxy is unknown, individually), we think it is premature to take this effect into account. Therefore, we consider the amplification of source only by the cluster, and assumed that J1 complex is the true optical counterpart of SMM J14011+0252.

private communication). No signature of AGN is found (e.g. Chapman et al. 2003c; Bower et al. 2004).

A5 A submm-detected faint 6.7 μm galaxy

The SCUBA observations in the field of very deep 6.7 μm survey (1σ sensitivity of 3 μJy) with *ISO* result in the detection of 3 submm sources (Sato et al. 2002). We collect SMMJ131225.7+424350 for which the spectroscopic redshift is available (Sato et al. 2002, 2004).

A6 GRB host Galaxies

Recent follow-up observations of γ -ray bursts (GRBs) at submm/radio wavelengths indicate that about 20% of GRB host galaxies are ULIRGs (Berger et al. 2003). Here we analyse three GRBs with the spectroscopic redshift; i.e. GRB 000210, GRB 000418 and GRB 010222 at $z = 0.846$, 1.119 and 1.477, respectively. All GRB hosts are detected not only at submm, but also at radio wavelengths, and therefore the optical identification is reliable (Frail et al. 2002; Berger et al. 2003).

APPENDIX B: ERROR ESTIMATES OF THE SED FITTING

In Figure B1, we show contour maps of $\Delta\chi^2$ for the sample used in Section 4, in which $\Delta\chi^2 = 1.0$, 2.71, and 6.63 correspond to the probability of 68.3 %, 90 %, and 99 %, respectively, when projected to each axis, i.e. t/t_0 and Θ . In most cases, the contour is elongated along the axis for the starburst age. However, note that the range of the starburst age within the confidence level of 68.3 % is reasonably small.

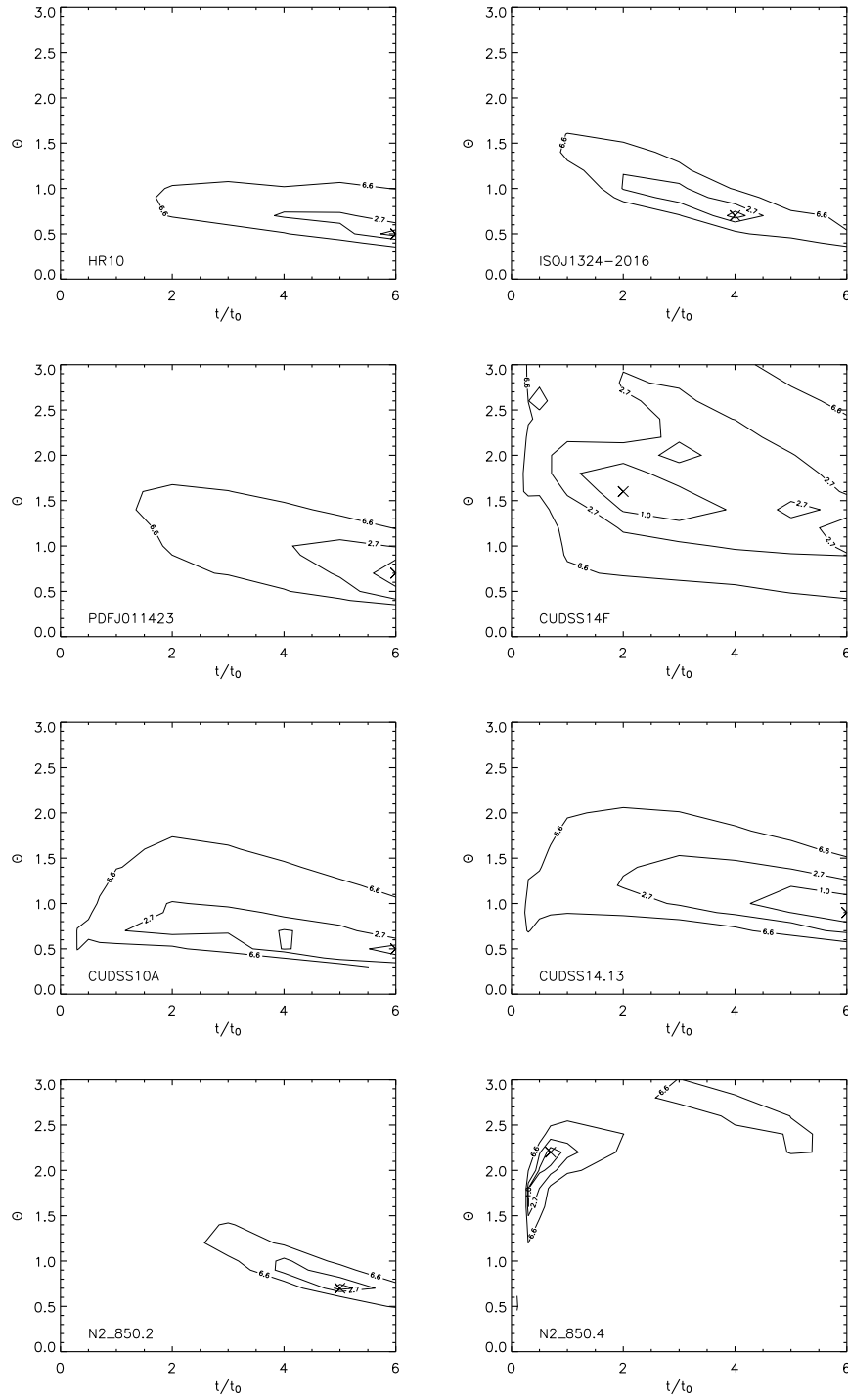


Figure B1. The contour maps of $\Delta\chi^2$ for the sample used in Section 4. The contours are depicted at $\Delta\chi^2 = 1.0$, 2.71, and 6.63, which correspond to the probability of 68.3 %, 90 %, and 99 %, respectively (when projected to each axis).

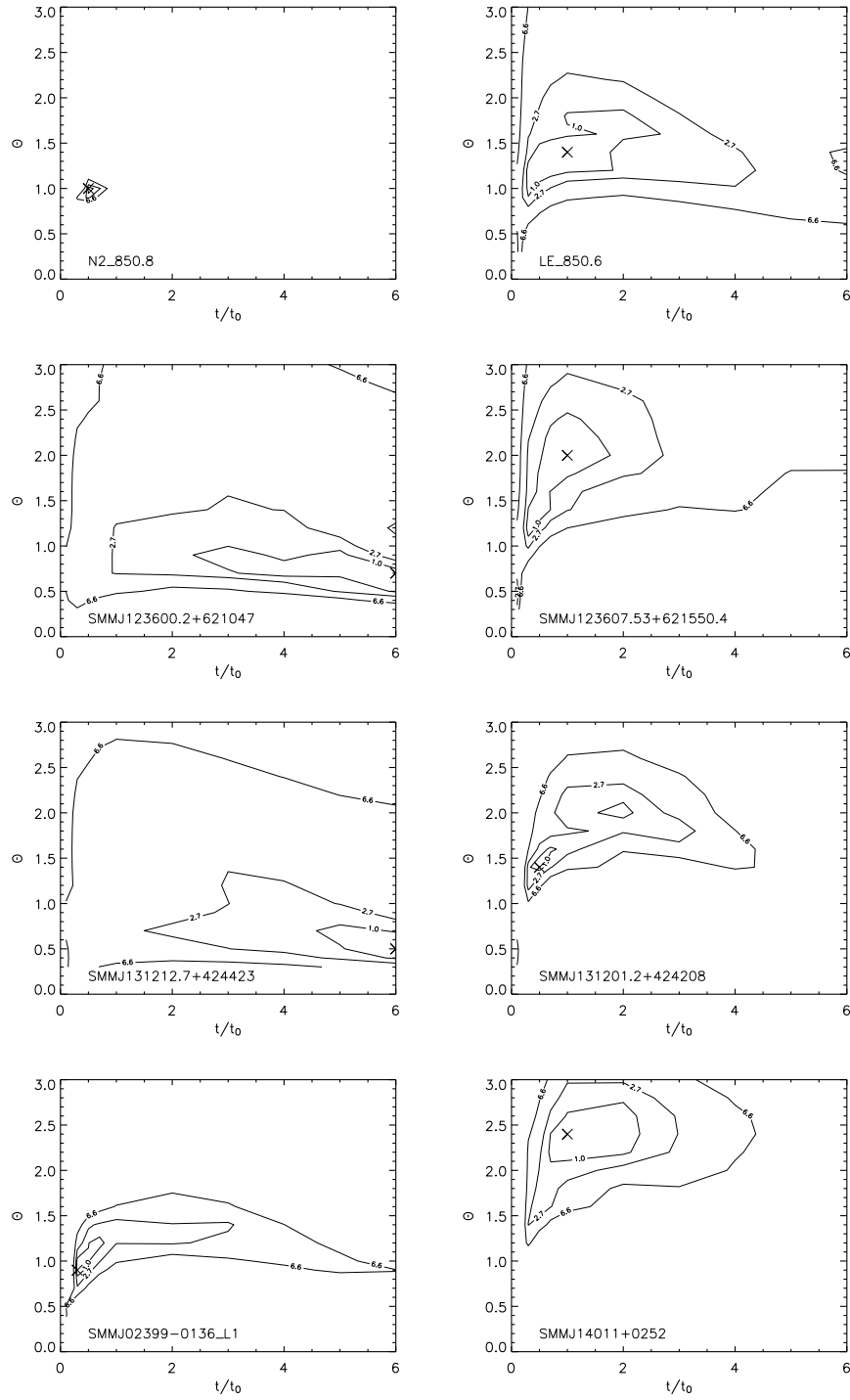


Figure B1. - *continued.*

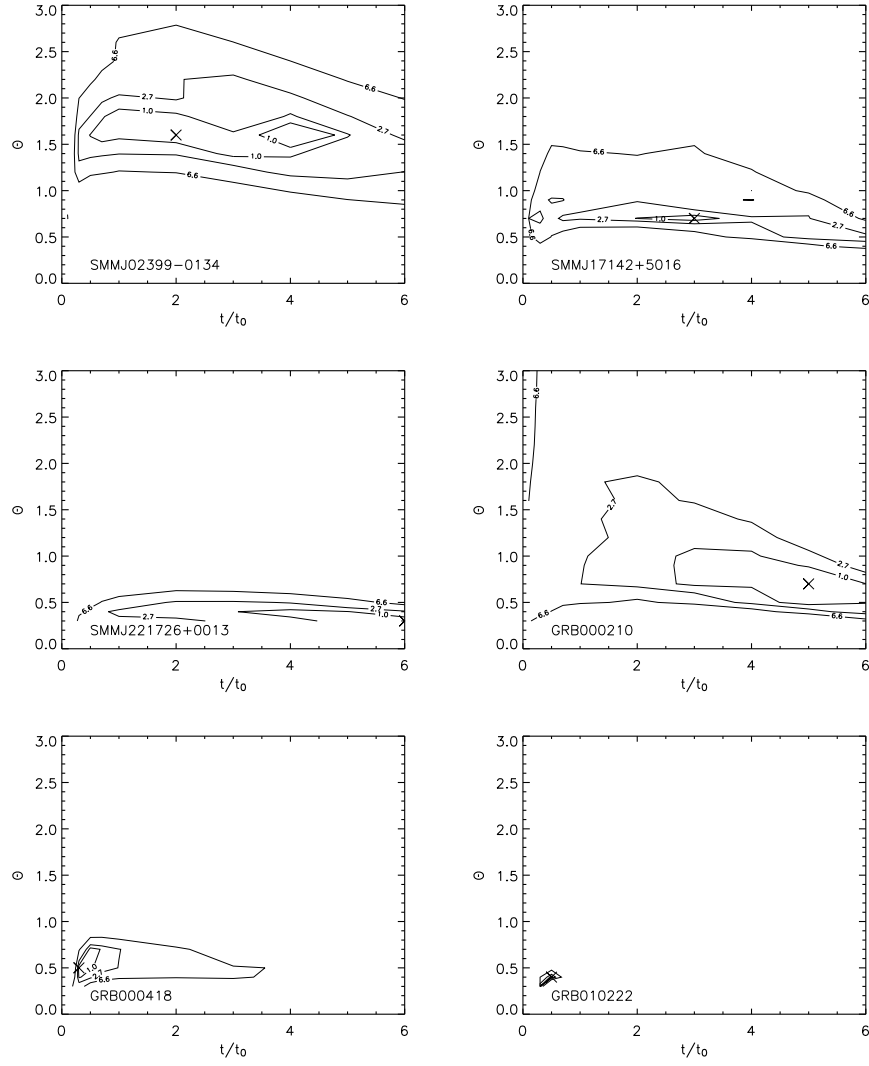


Figure B1. - continued.